<u>**İSTANBUL TECHNICAL UNIVERSITY ★ INFORMATICS INSTITUTE**</u>

**NON-NEWTONIAN BLOOD FLOW SIMULATION
IN A REALISTIC ARTERY**

**M.Sc. Thesis by
Hasret TÜRKERİ**

**Department :  Computational Science And Engineering**

**Programme :  Computational Science And Engineering**

**Thesis Supervisor: Prof. Dr. M. Serdar ÇELEBİ**

**MAY 2010**

**İSTANBUL TECHNICAL UNIVERSITY ★ INFORMATICS INSTITUTE**

**NON-NEWTONIAN BLOOD FLOW SIMULATION
IN A REALISTIC ARTERY**

**M.Sc. Thesis by
Hasret TÜRKERİ
(702071009)**

**Date of submission :   07 May 2010
Date of defence examination:   10 June 2010**

**Supervisor (Chairman) :   Prof. Dr. M. Serdar ÇELEBİ (ITU)
Members of the Examining Committee :   Prof. Dr. Nüzhet  DALFES (ITU)
Prof. Dr. Ömer GÖREN (ITU)**

**MAY 2010**

# İSTANBUL TEKNİK ÜNİVERSİTESİ ★ BİLİŞİM ENSTİTÜSÜ

## GERÇEK BİR DAMAR İÇİNDE NEWTONIAN OLMAYAN KAN AKIŞI BENZETİMİ

**YÜKSEK LİSANS TEZİ**
**Hasret TÜRKERİ**
**(702071009)**

**Tezin Enstitüye Verildiği Tarih :   07 Mayıs 2010**
**Tezin Savunulduğu Tarih :   10 Haziran 2010**

**Tez Danışmanı :   Prof. Dr. M. Serdar ÇELEBİ (İTÜ)**
**Diğer Jüri Üyeleri :   Prof. Dr. Nüzhet DALFES (İTÜ)**
**Prof. Dr. Ömer GÖREN (İTÜ)**

**MAYIS 2010**

## FOREWORD

I would like to thank Prof. Dr. M. Serdar Çelebi for being my advisor and mentor during this research.

Next, I would like to express my deep appreciation to Şenol Pişkin who have kindly shared his knowledge and wisdom with me.

Also, I would like to extend my thanks to my friends, Yasemin Dönmezer, Gülnur Demir, Esra Baltaoğlu, Birkan Tunç, Erke Arıbaş, Ahmet Tuncer Durak and my friends to the ones whose names I may have forgotten.

Finally, I would like to express my greatest gratitude to my family and their love over so many years.

May 2010                                              Hasret Türkeri

                                                     Mathematical Engineer

**TABLE OF CONTENTS**

## ABBREVIATIONS

| | |
|---|---|
| **RBC** | **:** Red Blood Cells |
| **WBC** | **:** White Blood Cells |
| **NP** | **:** RBC suspended in normal Plasma |
| **NA** | **:** RBC suspended in albumin |
| **HA** | **:** Hardened RBC suspended in albumin |
| **GPM** | **:** Generalised Power Method |
| **CT** | **:** Computed Tomograghy |
| **MRI** | **:** Magnetic Resonance Imaging |
| **FEM** | **:** Finite Element Methods |
| **CFD** | **:** Computational Fluid Dynamics |
| **FSI** | **:** Fluid Structure Interaction |
| **WSS** | **:** Wall Shear Stress |

**LIST OF TABLES**

## LIST OF FIGURES

# NON-NEWTONIAN BLOOD FLOW SIMULATION IN A REALISTIC ARTERY

## SUMMARY

In the literature blood flow simulations are studied frequently in order to understand the occurance of the diseases related to the blood flow and blood vessels. In these studies some assumptions are made because of the complexity of the physiology and vessel geometries. The most common used assumption is that viscosity of blood can be considered as constant on whole blood flow. However, blood has a complex structure and although this assumption may be convenient in some cases, the blood viscosity cannot be represented by constant viscosity.

The effects of the non-Newtonian viscosity and the outcomes of the assumption of being Newtonian are studied in the literature. In the studies, non-Newtonian and Newtonian models are simulated on a particular geometry and under particular flow conditions and the results of these cases are compared and discussed. Generally, the effect of non-Newtonian property depends on the flow geometry and the flow condition; such as Reynolds number, Womersly numbers, e.g.. Some of these studies indicate that the non-Newtonian properties have significant effect, so they must be considered on the simulation. On the other hand, some of these indicates that the non-Newtonian effects are not important and they may be ignored on the studies.

At present study, the effects of non-Newtonian viscosity are investigated on a realistic arterial domain. The used geometry was reconstructed from human CT data. Three dimensional Navier Stokes equation with three different non-Newtonian viscosity models; Casson, Carreau and Generalised Power Method is solved using finite volume method. At the input of the common carotid artery, experimental flow data which were obtained from a real artery bifurcation inlet are used. The response of vessel wall to the blood flow is also considered. The vessel wall is taken into account as isotropic and linear elastic material. The results of viscosity models in each cases, rigid wall and moving wall, are compared and discussed. The results

show that non-Newtonian viscosity has significant importance on WSS and velocity distribution at low Reynolds number.

## GERÇEKÇİ DAMAR ÜZERİNDE NON-NEWTONIAN KAN ALKIŞI BENZETİMİ

## ÖZET

Kan akışı ve damarlarla ilgili hastalıkların oluşumunu anlayabilmek amacıyla kan akışı simülasyonları literaturde sıkça çalışılmaktadır. Bu çalışmalarda birtakım kabuller yapılmaktadır. Bu kabullerin en önemlisi kanın Newtonian olduğu kabulüdür. Bu kabül ile kanın viskozitesi sabit kabul edilmektedir. Ancak kan kompleks bir yapıya sabittir ve sabit bir viskozite ile temsil edilmesi bazı durumlar için uygun görülebilir olmasına rağmen bazı durumlarda uygun değildir.

Literaturde kanın viskozitesi üzerine yapılan kabullerin sonuçlarını inceleyen birçok çalışma yapılmıştır. Bu çalışmalarda bazı non-Newtonian modeller ile simulasyonlar yapılarak Newtonian durumu ile karşılaştırılmıştır. Bu karşılaştırmalar sonucunda birtakım değerlendirmeler yapılmıştır. Bu değerlendirmeler, simulasyonun yapıldığı geometriye, akış özelliklerine, akış hızına v.b. gibi özelliklere bağlı olarak değişiklik göstermektedir. Bazı çalışmalar non-Newtonian özelliklerin çok önemli olduğunu ve kan akışı simulasyonlarında ihmal edilmemesi gerektiğini vurgularken, bazı çalışmalar non-Newtonian özelliklerin ihmal edilebilir etkilere sahip olduklarını söylemektedirler.

Bu çalışmamızda non-Newtonian özelliklerin etkileri gerçekçi atardamar geometrisi üzerinde incelenmektedir. Kullanılan geometri insan CT verisinden elde edilmiştir. Üç boyutlu Navier Stokes denklemi üç farklı non-Newtonian model; Carreau, Casson ve Generalised Power method ve Newtonian viscosity modeli ile birleştirilerek çözüldü. Ayrıca bu çalışmada damar çeperlerinin akışkana olan etkileri de göz önüne alınmıştır. Damar duvarı hem sabit hemde hareketli olduğu durumlarda simulasyon yapılarak her iki durum için de non-Newtonian etkiler incelenmiştir. Damar duvarının hareketli kabul edildiği durumda, damar duvarı doğrusal elastic, izotropik özelliklere sahip olduğu kabul edilmiştir. Sonuçlar düşük Reynold sayılı akışlarda non-Newtonian özelliklerin önemli etkilere sahip olduklarını göstermektedir.

# 1. INTRODUCTION

Human body has a complex structure. The complexity of human body complicates conducting studies on investigating the human physiology. Both biomechanical and biofluid studies suffer from the complexity of the human body. Thus, having some assumptions and constraints becomes an obligation when working on any subsystem of the human body, especially with the blood flow. Although the vessel wall is porous media, heterogeneous and highly viscoelastic material, it is assumed as rigid wall. Furthermore, human blood is multi-phase fluid, but it is considered as homogenous fluid. Moreover, while the vessel wall moves due to the pulsatile flow, the vessel wall is assumed as motionless. In addition to this, one of the most common assumption used in the simulations is simplification of the arterial domain which has a complex geometry. Another assumption used in the studies is on the rheological properties of the blood such that the viscosity of blood is considered as being Newtonian. While the assumptions make the studies of blood flow handleable, the accuracy of the studies damage.

In the literature, several blood flow simulations are conducted to investigate the basics of blood flow in arteries, and to understand the construction of diseases relevant to blood flow. In these studies some assumptions are made because the blood flow simulation has difficulties due to the small size of vessel and the complex structure of blood. The most applied assumption about the structure of blood is that the blood viscosity can be describe as being Newtonian due to the having constant apparent viscosity above $100s^{-1}$ in large arteries. However, the strain rate of blood flow is not above $100s^{-1}$ in some regions or at some instants therefore, the assumption of being Newtonian may underestimate the flow properties on these regions and at these instants.

In the present study, the effects of the assumptions on the structure of blood, on the blood flow simulations are investigated. The assumptions are assessed by using three viscosity models namely; Carreau, Casson, and Generalised Power Method, as well

as Newtonian model in the simulations, and comparing the results of wall shear stress distributions and velocity profiles of each case.

The characteristics of viscosity models are investigated on the various flow conditions at a realistic artery domain. Steady and unsteady simulations are conducted with rigid vessel wall assumption. Furthermore, unsteady simulation is done with moving vessel wall boundary. The blood and vessel wall interaction is achieved by loosely coupling the both fluid and structural software. The results of the flow properties at each flow condition are compared and discussed.

## 2.  LITERATURE REVIEW

The blood flow simulations are studied to understand the occurrence of the diseases and the anomaly in blood flow in artery. Although, the blood flow simulations are studied in literature exhaustively, there is no generally accepted viscosity model that represents the behavior of blood rheology efficiently. Some studies assume the blood as Newtonian while some of them assume the blood as non-Newtonian. Moreover, there are various non-Newtonian viscosity models, which derived using parameter fitting.

In literature, many studies are conducted to analyse the effects of the viscosity models numerically or experimentally. Some of these studies indicates that non-Newtonian properties have significant role while some studies implies that non-Newtonian properties have minor importance.

To quantify the importance of non-Newtonain models on anastomotic flow patterns, the characteristics of Newtonian and non-Newtonian blood flows are compared in a 2-D, $45°$ end-to-side anastomosis model under steady and unsteady flow conditions [1]. The study indicates that non-Newtonian blood has a significant effect on steady flow wall shear stresses, but only minor effect on unsteady flow wall shear stresses. It is concluded that non-Newtonian viscosity effects in the distal circulation are of secondary importance.

An idealised, $45°$ rigid, 6 mm diameter, end-to-side femoral anastomosis was modeled to investigate the effects of non-Newtonian rheology of blood [2]. A steady flow with 0.15 and 0.01 m/s inlet velocities was simulated to model high and low wall shear stresses respectevely. While at high shear rates there was no significant difference between WSS distribution, at low shear rates there were qualitative differences of up to 300%. It was concluded that the choice of viscosity model has to be based on the situation under study, e.g flow rate, steady/unsteady flow, and geometry.

The influence of viscoelastic effects on blood flow in large arteries is investigated using the Jeffreys' type (Oldroyd-B) and Casson models [3]. Whereas Oldroyd-B describes the viscoelastic properties of blood, Casson describes the shear thinning properties. The effects are studied on the steady flow through a tree-dimensional axisymmetric tube with a stenosed, and a curved tube. The numerical results indicate significant influence of viscoelastic effects in the stenosed model. On the flow through the curved tube the effects of viscoelastic properties is minor important. Moreover, the shear thinning effect can be observed in both geometries. The study indicates that the influence of viscoelastic properties in large arteries depends on the shape of the flow domain.

A comparative study of non-Newtonian and Newtonian models is carried out [4]. In the study, two non-Newtonian; the Power law and Casson models, and Newtonian model are used to simulate unsteady flow through a hypothetical stenotic geometry. Through comparison of the results the three models, it was found that the wall shear stress distribution for Newtonian model has the lowest value. However, the peak wall shear stress gradient for Power law is the highest. Flow characteristics such as higher pressure drop across the stenosis, location and movement of vortex are similar in all three models. It is pointed out that the effects of Non-Newtonian are more significant in the vicinity of the stenosis.

Effects of the non-Newtonian viscosity of blood on flow in a coronary artery are studied [5]. In this stdy, the pressure drop, wall shear stress and velocity profiles for the case of blood viscosity were compared for the case of Newtonian viscosity. The effect of the non-Newtonian viscosity of blood on overall pressure drop across the arterial casting was flound to be significant at a flow of the Reynolds number of 100 or less. In the region of flow separation or recirculation, the non-Newtonian viscosity of blood yields larger WSS than the Newtonian case.

A study in a stenosed artery incorporating fluid-structure interaction is implimented [6]. In the study, the wall is considered as isotropic and elastic. The artery geometry was modeled as an axisymmetric stenosed vessel. The blood behavior described by the non-Newronian models (Power Law and Carreau) and Newtonian model. While the Carreau model showed only slightly smaller centreline axial velocities, the Power Law model showed more significant differeces, including flatter velocity profile. The WSS distributions show similar trends except the Power Law model shows

significantly smaller magnitudes. Moreover, the Carreau model exhibits slightly larger stresses.

The study on aneurysmal wall is carried out to investigate the effect of non-Newtonian models [7]. The geometry is constructed from angiography image data and the flow is considered as unsteady laminar flow in this study. The study indicates that the predictions with the Newtonian and non-Newtonian blood models are similar and the effect of the non-Newtonian properties of blood on the WSS is important only in the arterial regions with high velocity gradients.

In two dimensional blood flow which interact with compliant vessel [8]. Carreau and Yeleswarapu models used to presents the shear-thinning property of blood. The result was shown that there are only marginal differences in the WSS between non-Newtonian models. On the other hand, the differences between the Newtonian and non-Newtonian models are more visible.

The non-Newtonian effects were investigated on coronary bypass anastomosis [9]. In the study, a simplified geometry of end-to-side coronary bypass anastomosis is considered. The coronary artery has a 75% severity stenosis. The results shows that significant differences in axial velocity profiles, secondary flow streamlines and WSS between the non-Newtonian and Newtonian fluid flows are revealed. In the study, it is concluded that non-Newtonian property of blood alters the flow pattern and WSS distribution and is an important factor to be considered in simulating hemodynamic effect of blood flow in arterial bypass grafts.

A comparison of non-Newtonian and Newtonian models was made on a bifurcation model with a non-planar daughter branch [10, 11]. In the study, the flow was considered as pulsatile flow, and for the non-Newtonian model, the Carreu-Yasuda model was used to take into account the shear thinning behavior of tha analog blood fluid. In the daughter vessel the non-Newtonian model result in flattened axial velocity due to the its shear thinning behavior. Moreover, significant difference between the non-Newtonain and the Newtonian flow was found. The study indicates that the non-Newtonian properties of blood is an important factor in hemodynamics and may play a significant role in vascular biology and pathophysiology.

A study in which three non-newtonian models (Casson, Walburn-Schneck and Generalized Power Law) is carrried out to investigate the impact of the blood models

in an anatomically realistic model of the left coronary artery main bifurcation [12]. In the study, it was found that the WSS is influenced by the used model. Moreover, only the Walburn-Schneck model revealed significant varied WSS distribution if compared with Newtonian model. In this study it was concluded that the impact of the non-Newtonian blood model in WSS profiling of coronary artery flow may be neglected for clinical studies with normal or narrowed coronary arteries. However, for dilated coronary arteries, the non-Newtonian blood model is significant and should be included in numerical model of the coronary flow.

A study on the flow behavior of blood through a porous medium stenosed artery and to investigate the significance of the non-Newtonian effects on bood flow is implemented [13]. The goemetry has stenosis severity ranging from 25% to 80%, is a straight tube of length of 5 cm and diameter of lumen is 0.21cm. The study indicates that the non-Newtonian model has significant effects on the velocity profile and the magnitude of the WSS.

By taking turbulence effects into account, an investigation of effects of non-Newtonian blood model is carried out [14]. In this study, the realistic pulsatile flow was used, and the geometry was simple vessels of actual size. Comparisons were made between non-Newtonian and Newtonian blood model on pressure, strain rate and velocity component distributions. Significant disaggrement between non-Newtonian and Newtonian models were found. In this study, it is concluded that those models not using non-Newtonian models underestimate the risk of disruption to the human vascular system.

To assess the effects of non-Newtonian model, the lattice Boltzmann method was modified and used [15]. Two non-Newtonian models (Casson and Carreau-Yasuda) as well as Newtonian model were considered in the two-dimensional flow in context of simple steady flow and oscillatory flow in straight and curved pipe. Significant difference between non-Newtonian and Newtonian models was present in the steady flow simulation. In the oscillatatory flows, non-Newtonian models exhibit significant differences at low Reynolds and Womersley numbers. In the study it was concluded that these differences may be important for the study of atherosclerotic progression.

Five non-Newtonian models, Casson, Carreau, Generalised Power Method, Power Method and Walburn-Schneck, were used and compared based on WSS distribution in a steady-state simulation [16]. Initial results reveal that for a low central inlet

velocity, WSS values of non-Newtonian models are higher than that of Newtonian. In the case of high central inlet velocity, WSS values of non-Newtonian and Newtonian models are nearly identical while the WSS of Power Law and Walburn-Schneck are lower than that of others. In the subsequent study of these authors, Generalised Power Method and Newtonian method were compared in transient simulation [17]. Results show that the difference between distributions of WSS in Generalised Power Method and Newtonian Method is relatively small.

Experimental and numerical studies were performed to investigate the effect of influence of the non-Newtonian properties on the velocity distribution [18]. In the study, steady flow in a three dimensional model of the carotid bifurcation was carried out. In this study it is indicated that significant differences between the Newtonian and non-Newtonian fluid are present. While the axial velocity profile for the Newtonian fluid is parabolic, the velocity profile of the non-Newtonian fluid is flattened. In the numerical simulation viscoelasticity property of blood was not considered, but only shear-thinning property was taken into account numerical results are well agreed with the experimental results. Since the numerical results and experimantel results are well agreed, it can be inferenced that the shear-thinning properties are the dominant non-Newtonian property of the blood.

In a two dimensional human carotid artery bifurcation, the stationary flow of blood is simulated using Casson, Power-law and the Newtonian viscosity models [19]. The simulation is carried out using Reynolds number which taken as equal to 300. The velocity profiles of non-Newtonian models have 5-10% lower maximum values compared to the Newtonian model. The pressure non-Newtonian has higher values up to 25% than that of the Newtonian model. The generalized Newtonian models give higher wall shear stress along the non-divider wall than the Newtonian model, the maximum difference being 5%. From the results, it is concluded that the general flow structure is not influenced by the non-Newtonian models.

## 3. BLOOD RHEOLOGY

### 3.1 Blood Composition and Structure

Blood has a complex structure with multi-phase fluid and composed of suspended elements in plasma which is continuous part of blood. It's components are 91% water, 7% proteins, 2% inorganics and other organics solutes. The proteins include fibrinogen, globulins, albumin, beta lipoprotein and lipalbumin. The proportions of first three proteins are 5%, 45% and 50% in plasma protein respectively. Beta lipoprotein and lipalbumin are in very small proportions. Plasma can be considered as a Newtonian fluid which has a viscosity about $1.2 \, \text{mPa} \cdot \text{s}$ at $37 \, ^\circ\text{C}$.

The White Blood Cells (WBCs) have major role in defense of body. It is known that the platelets have mission in clotting process. The concentrations of WBCs and platelets are fewer compared to the Red Blood Cells (RBCs). Therefore, the effects of WBCs on blood flow are negligible.

The Red Blood Cells (RBCs) are biconcave discs with a diameter of approximate 8 $\mu \cdot \text{m}$ (see Figure 3.1). The volume of the typical RBC is approximately 85 to 90 microns. The RBCs have a very flexible membrane enclosing hemoglobin solution. The viscosity of hemoglobin is about $6 \, \text{mPa} \cdot \text{s}$ which five times larger that of blood. Because of having the elastic membrane and highly viscous hemoglobin solution, the RBCs have abilities to deform themselves. The property of deformability enables the RBCs not only to pass through capillaries ($5 \, \mu\text{m}$ in diameter), but also through the endothelial wall. Hematocrit is used to represent the volume friction in plasma. It is known that the hematocrit has significant role to determine the blood viscosity. Its normal range is about 47% in adult male and about 42% in adult female.

Aggregation behavior of the RBCs is the most important characteristic acting on the blood viscosity. The RBCs tent to come together and form rouleaux at low shear rate. The fibrinogen in plasma have active role in aggregation. At rest state, the RBCs constitute one big aggregation which likes a solid. When a limiting shear stress, yield stress, is exceeded, the aggregation begins to break up. Then it occurs clusters of

rouleaux in plasma as shown in Figure 3.2. Between the size of aggregation and the shear stress, there is a dynamic equilibrium. At the high shear rates which above $100 \text{ s}^{-1}$, aggregates are reduced to individual cells, and RBCs are deformed into ellipsoid with their long axes aligned in the direction of flow.
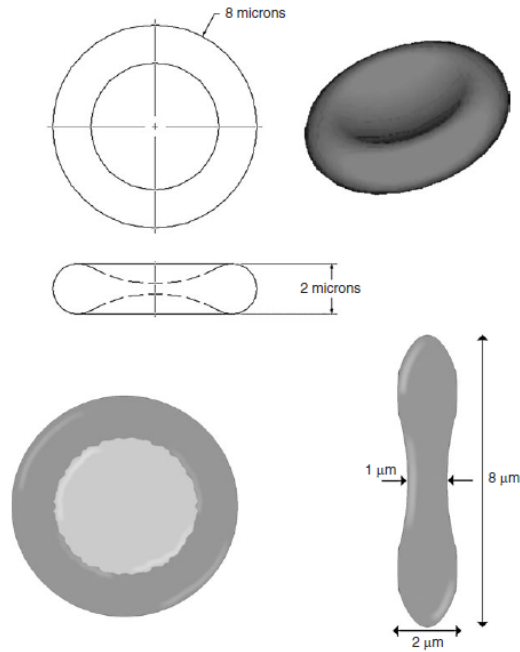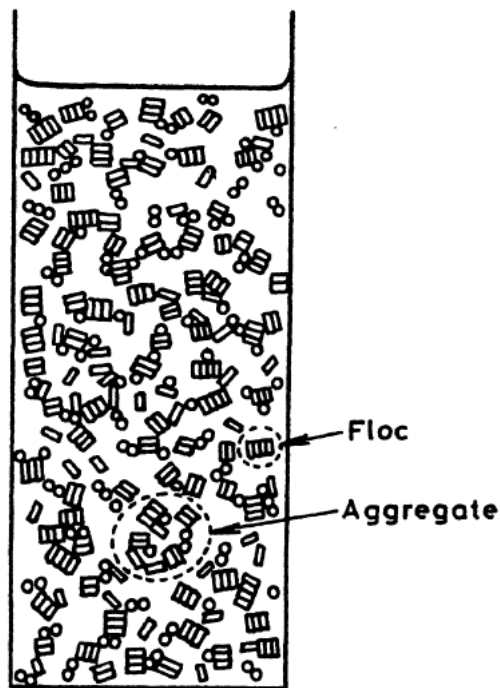


**Figure 3.1 :** Shape of Red Blood Cells



**Figure 3.2 :** Aggregation of RBCs

## 3.2 Blood Viscosity

Temperature is an important parameter for blood viscosity. Between fall in temperature and rise in viscosity there is a linear relationship within the range of $27\text{-}37°C$. Plasma viscosity increases rapidly as the temperature falls below $27°C$.

In Figure 3.3, the relationship of viscosity of three types of RBCs between are illustrated. The types of RBCs are RBCs suspended in normal plasma (NP), RBCs suspended in albumin (NA), and hardened RBCs in albumin (HA). The albumin can be used to prevent the RBCs to aggregate therefore, the RBCs in albumin are individual cells. Moreover, hardened RBCs in albumin are prevented to deform. In this way, the effect of aggregation and deformation of the RBCs on the blood viscosity are clarified. The difference between NP and NA curves show the effect of cell aggregation, whereas the difference between NA and HA indicates the effect of cell deformation. Aggregation of red cells at low shear rates causes to increase of viscosity. The deformation at high shear rates leads to decrease of viscosity. Moreover, the viscosity hardened RBCs suspension is independent of shear.



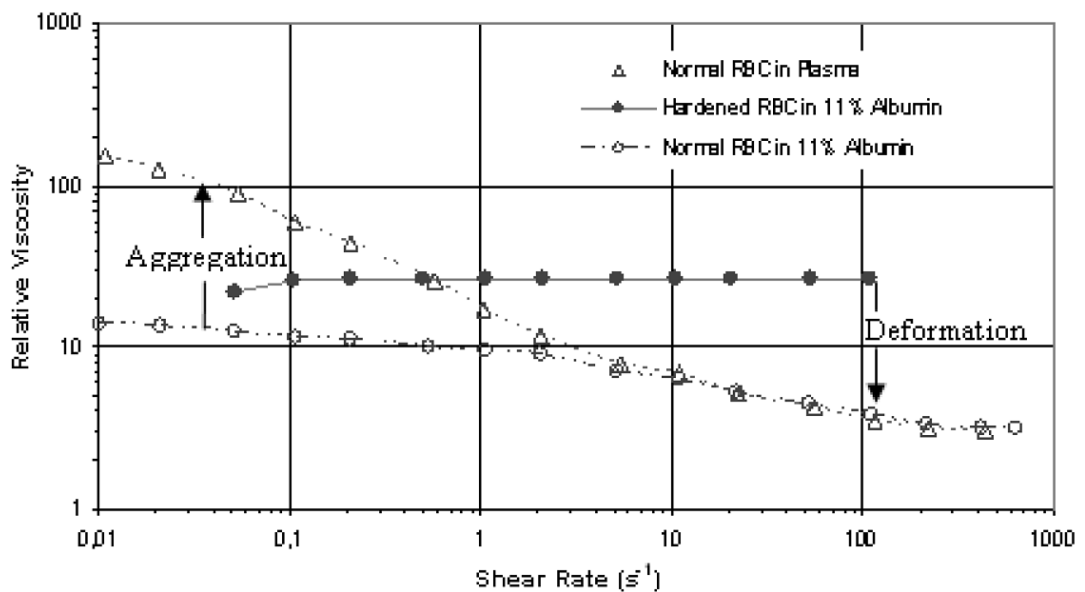**Figure 3.3 :** Relation between relative viscosity and shear rate in three types of RBCs suspensions

When blood flow through vessels smaller than about 1.5 mm in diameter, the apparent viscosity of the fluid decrease. This effect is known as the *Fahraeus-Lindqvist* effect. Figure 3.4 shows that the viscosity is a function of vessel diameter. While the diameter of vessel decreases, viscosity of blood decreases. However, when

the diameter of the vessel closer to the diameter of the RBCs, the viscosity increases dramatically.
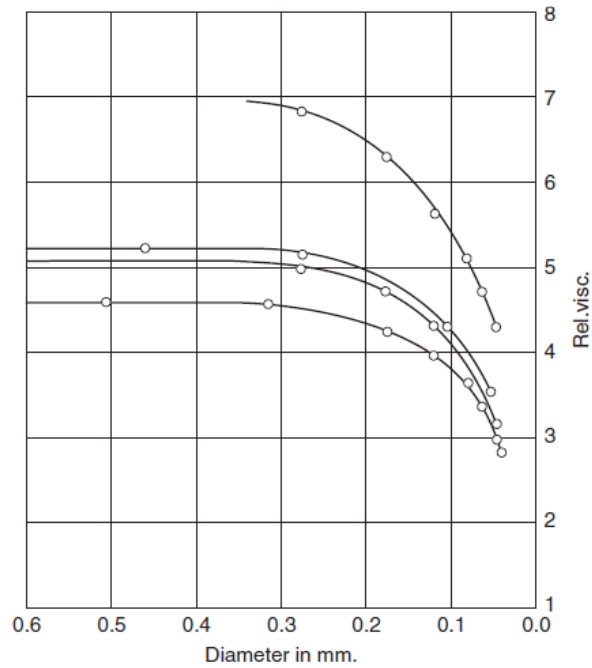


**Figure 3.4 :** Fahraeus-Lindqvist Effect in the blood vessel

The viscosity of blood is also a strong function of hematocrit, or volume percent of RBCs. Figure 3.5 shows the relationship between blood viscosity and hematocrit with the range from 0 to 0.65.
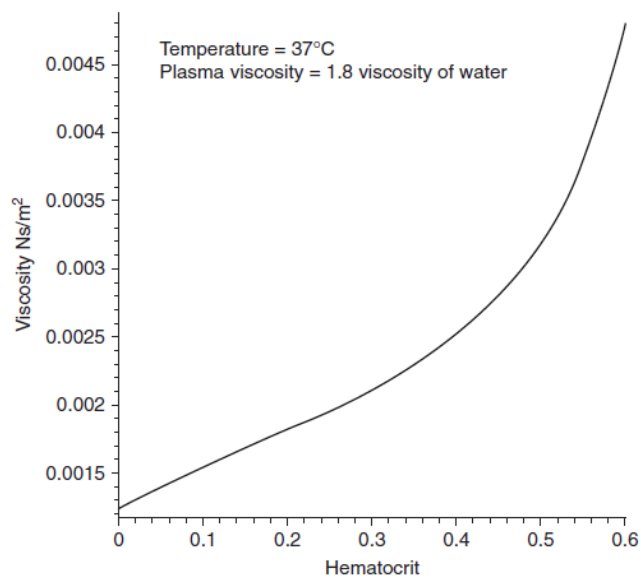


**Figure 3.5 :** The relationship between Hematocrit and Blood Viscosity

11

### 3.3 Mathematical Models of Blood Viscosity

Blood flow exhibits non-Newtonian behavior such as shear thinning, thixotropy, viscoelasticity, and yield stress. It's viscosity is effected by many factors such as plasma viscosity, aligment of RBCs, level of RBC aggregation and deformation, fibrinogen, flow geometry and size, rate of shear, hematocrit, male or female, smoker or non-smoker, temperature, lipid loading, hypocaloric diet, cholesterol level, physical index, diabetes mellitus, arterial hypertension, sepsis, etc.. Blood viscosity model in the literature may be group into two categories such as Newtonian viscosity and non-Newtonian viscosity.

### 3.3.1 Newtonian viscosity

The blood can be assumed as a Newtonian fluid when shear rate over a limiting value. In literature, there is a variation on the limiting shear rate. In some studies, the limiting shear rate is considered on the range from $50 \text{ s}^{-1}$ to $100 \text{ s}^{-1}$ whereas in others, this range is considered as from $100 \text{ s}^{-1}$ to $300 \text{ s}^{-1}$. At high shear rates in large arterial vessel which has diameter greater than 1mm, blood viscosity is modeled as constant value. The constant value is assumed as the value of high limiting viscosity of blood which generally accepted as $3.5 \text{ mPa} \cdot \text{s}$.

### 3.3.2 Non-Newtonian viscosity

Due to the variations on the shear rate which approximately from zero to $1000 \text{ s}^{-1}$ over a cardiac cycle in large arteries, the blood exhibits shear thinning behavior. In addition to this, at low shear rate zones such as near bifurcations, graft anastomoses, stenoses, and aneurysm, the blood exhibits non-Newtonian properties. To model the shear thinning properties of blood, various non-Newtonian blood models are constituted in the literature.

The apparent viscosity of blood have three distinct region, namely lower Newtonian region which has a constant viscosity, $\mu_0$ at lower shear rate, upper Newtonian region which has a constant viscosity, $\mu_\infty$ at higher shear rates and middle region where the apparent viscosity is decreasing with the increasing shear rate.

Casson considers the effect of the RBC concentration. Generalised Power Law model consists of the Power Law model at low strain, the Newtonian model at mid-

range and the Casson model at high strain rates. The Carreau model takes both $\mu_0$ and $\mu_\infty$ into account to consider the limiting values of viscosity where $\mu_0$ is the limiting viscosity while shear rate tends to zero and $\mu_\infty$ is the limiting viscosity while the shear rate goes to infinity.

**Table 3.1:** Mathematical Models of Blood Viscosity

| Model Name | Viscosity Model |
|---|---|
| Newtonian model | $\mu = 0.00345$ P |
| Carreau model | $\mu = \mu_\infty + (\mu_0 - \mu_\infty)\left[1 + (\lambda\dot{\gamma})^2\right]^{(n-1)/2}$, <br><br> where $\lambda$=3.313s, n=0.3568, $\mu_0$=0.56 P and $\mu_\infty$=0.0345 P [5] |
| Casson model | $\mu = \left[\left(\eta^2 J_2\right)^{1/4} + 2^{-1/2}\tau_y^{1/2}\right]^2 J_2^{-1/2}$, <br><br> where $\|\dot{\gamma}\| = 2\sqrt{J_2}$, $\tau_y = 0.1(0.0625H)^3$, <br><br> $\eta = \eta_0(1-H)^{-2.5}$, $\eta_0 = 0.012$P, H=0.37 [20] |
| Generalised Power Law model | $\mu = \lambda\|\dot{\gamma}\|^{n-1}$, <br><br> $\lambda(\dot{\gamma}) = \mu_\infty + \Delta\mu\exp\left[-\left(1+\dfrac{\|\dot{\gamma}\|}{a}\right)\exp\left(\dfrac{-b}{\|\dot{\gamma}\|}\right)\right]$, <br><br> $n(\dot{\gamma}) = n_\infty - \Delta n\exp\left[-\left(1+\dfrac{\|\dot{\gamma}\|}{c}\right)\exp\left(\dfrac{-d}{\|\dot{\gamma}\|}\right)\right]$, <br><br> where $\mu_\infty = 0.035$ P, $n_\infty = 1.0$, $\Delta\mu = 0.25$, $\Delta n = 0.45$, <br> $a = 50, b = 3, c = 50$ and $d = 4$ [1] |

As it can be seen in Figure 3.5.a, the Generalized Power Method has a greater viscosity at low shear rate. The viscosity of Carreua and GPM models are close to each other for shear rate values over 0.2s. For high shear range, the GPM and Carreau models converge to a limiting value which is Newtonian viscosity. On the other hand, the viscosity of Casson model is smaller than that of others at low strain rate and above that of other models at high shear rates and it does not converge to the Newtonian viscosity at high shear rates. Figure 3.5.b shows that the shear stresses for non-Newtonian models are higher than that of Newtonian at low strain values. Furthermore, above $100 \text{ s}^{-1}$, the shear stress of non-Newtonian models converges to the Newtonian model.

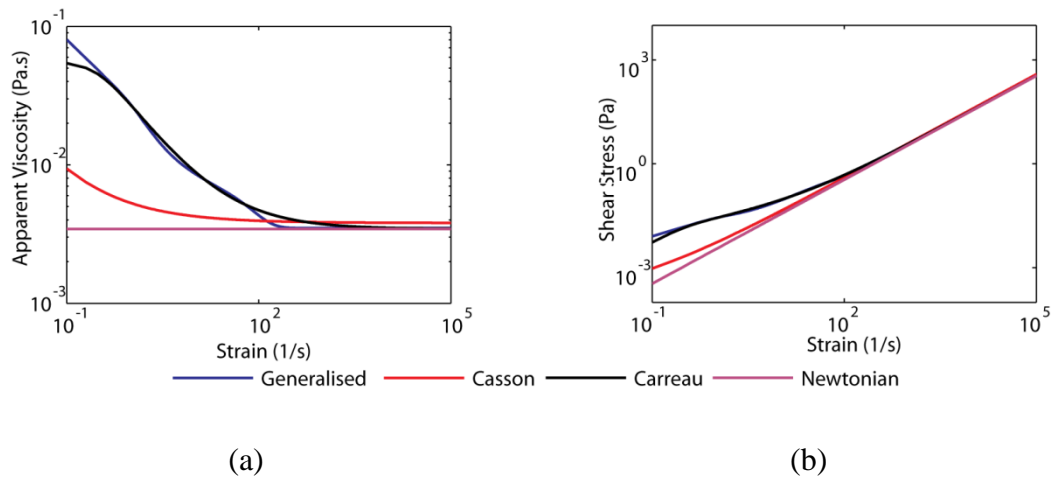|                |                |
| :------------: | :------------: |
| (a)            | (b)            |

**Figure 3.6 :** Apparent viscosity and shear stress as a function of strain (a) Viscosity (b) Shear Stress

## 4. NON-NEWTONIAN FLUID BEHAVIOUR

Blood is a non-Newtonian fluid whose flow curve (shear stress versus shear rate) is non-linear or does not pass through origin. At a given temperature and pressure, the apparent viscosity, shear stress divided by shear rate, is not constant. However, it depends on flow conditions such as flow geometry, shear rate, etc.. The non-Newtonian fluid may be grouped into three general classes:

1. Fluids for which the rate of shear depends only the value of the shear stress at that space and time. This type of fluid is known as "time independent fluids" or "generalized Newtonian fluids".

2. Fluids for which the rate of shear depends in addition upon the duration of shearing and their kinematic history. This type of fluid is called "time dependent fluids".

3. Substances exhibiting characteristics of both ideal fluids and elastics solids. This type of fluid categorized as "visco-elastic fluid".

### 4.1 Time-Independent Fluid Behaviour

In the simple shear, the flow behavior of time independent fluids may be described by a constitutive relation of the form,

$$\dot{\gamma}_{yx} = f\left(\tau_{yx}\right) \tag{4.1}$$

where $\tau$ is shear stress and $\dot{\gamma}$ is strain rate.

It can be inferred that the value of shear rate at any point is determined by only by the current value of shear stress at that point. These fluids may be further subdivided into three types according to the form of the function in Equation 4.1.

    a) Shear-thinning or pseudoplastic
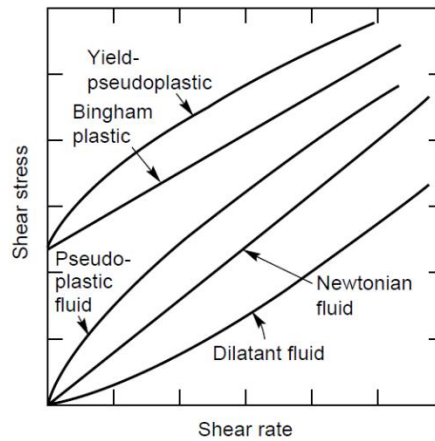
    b) Viscoplastic

    c) Shear-thickening or dilatants

**Figure 4.1 :** Types of time-independent flow behavior

### 4.1.1 Shear-thinning or pseudoplastic fluids

This type of non-Newtonian fluids is characterized by an apparent viscosity which decreases with increasing shear rate. Both at low and high shear rates, most shear-thinning fluids exhibit Newtonian behavior, apparent viscosity becomes straight lines. The resulting values of the apparent viscosity at very low and high shear rates are known as the zero shear viscosity, $\mu_0$, and the infinite shear viscosity, $\mu_\infty$, respectively. Therefore, the apparent viscosity of a shear-thinning fluid decreases from $\mu_0$ to $\mu_\infty$ with increasing shear rate.
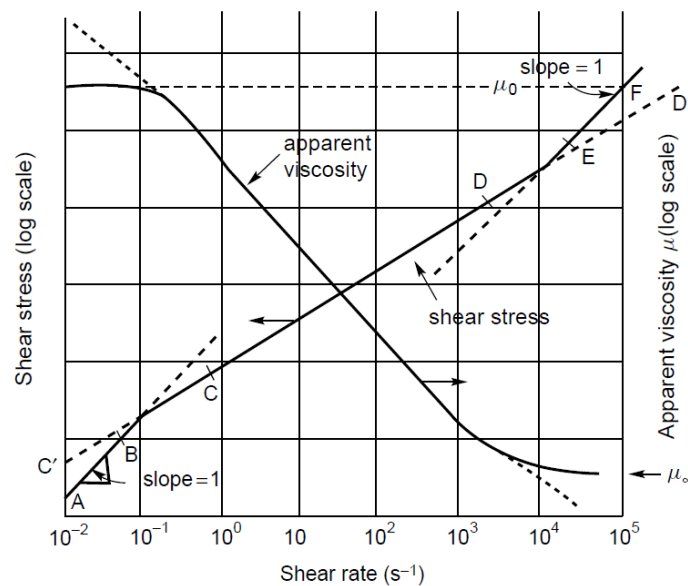


**Figure 4.2 :** Shear thinning behavior

16

### 4.1.2 Viscoplastic

The existence of a yield stress characterizes this type of fluids. The yield stress must be exceeded, before the fluid will deform or flow. When the magnitude of yield stress is exceeded the flow curve may be linear or non-linear but, it will not pass through origin as shown in Figure 4.3. Bingham plastic fluid has a linear flow curve for $\left|\tau_{yx}\right| > \left|\tau_0\right|$ and is characterized by a constant viscosity and a yield stress. Moreover, yield-pseudoplastic fluid has a yield stress and a non-linear flow curve. In addition to this, a viscoplastic fluid displays an apparent viscosity which decreases with the increasing shear rate.
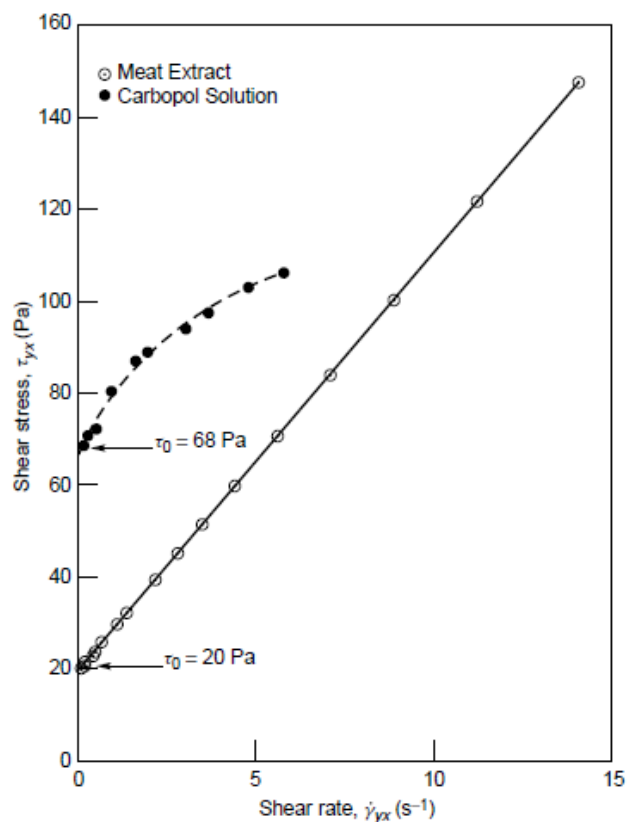


**Figure 4.3 :** Shear stress − shear rate relationship of Bingham Plastic and a carbopol polymer solution

### 4.1.3 Shear-thickening or dilatant fluid behavior

Dilatant fluids have apparent viscosity which increases with increasing viscosity and they have no yield stress as pseudoplastic fluids.

17

## 4.2 Time-Dependent Fluid Behaviour

The apparent viscosity of time-dependent fluid depends not only the rate of shear but also on the time for which the fluid has been subjected to shearing. Time-dependent fluid behavior may be sub-divided into two categories: thixotropy and rheopexy or negative thixotropy. For thixotropy fluid, the apparent viscosity decreases with the time of shearing when it is sheared at a constant rate. For rheopexy fluids, the apparent viscosity increases with time of shearing when it is sheared at a constant rate.

## 4.3 Viscoelastic Fluid Behaviour

Viscoelastic fluid is one whose property of material exhibits both viscous and elastic characteristics when external force applied. Viscous material resists to flow when a stress is applied. Elastic material strains and deforms themselves when stretched and once the external force is removed, elastic material returns to their original state.

## 4.4 Mathematical Model for Non-Newtonian Fluids

### 4.4.1 Power Law Method

The relationship between shear rate and shear stress for a shear-thinning fluid can be approximated by a straight line over a limited range of shear rate. On this part of the flow curve, the following expressing can be suitable:

$$\tau_{yx} = m\left(\dot{\gamma}_{yx}\right)^n \tag{4.2}$$

Hence, the apparent viscosity for the power law fluid given by:

$$\mu = \tau_{yx} / \dot{\gamma}_{yx} = m\left(\dot{\gamma}_{yx}\right)^{n-1} \tag{4.3}$$

The fluid exhibits shear thinning properties for n < 1, the Newtonian behavior for n = 1 and the shear-thickening behavior for n > 1. In Equation 4.2 *m* and *n* are two empirical curve-fitting parameters and are called as the fluid consistency coefficient and the flow behavior index respectively. For a shear-thinning fluid, the smaller the value of n, the grater is the degree of the shear-thinning. The Power Law Method is convenient over only a limited range of shear rates and therefore, the fitting

parameters depends on the range of shear rates considered. Moreover, the zero viscosity and infinite viscosity are not predicted as shown in the Figure 4.4.
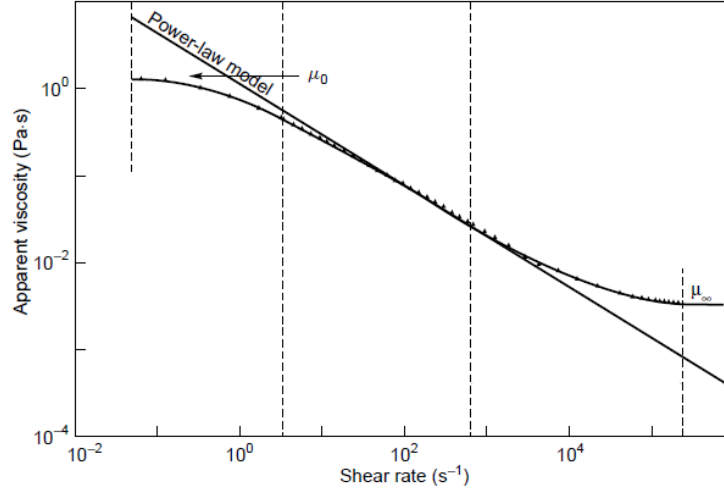


**Figure 4.4 :**Demonstration of zero and infinite shear viscosity for a shear-thinning polymer solution

### 4.4.2 Carreau Model

Carreau Model is a viscosity model for shear-thinning flud. Since the Power Law method does not consider the values of $\mu_0$ and $\mu_\infty$, at very low and very high shear rates, this model cannot describe shear thinning behavior. The Carreau model incorporates both limiting viscosities $\mu_0$ and $\mu_\infty$ as the following form:

$$\frac{\mu - \mu_\infty}{(\mu_0 + \mu_\infty)} = \left[ 1 + (\lambda\dot{\gamma})^2 \right]^{(n-1)/2} \tag{4.4}$$

where $n(<1)$ and $\lambda$ are two curve-fitting parameters. This model can represent shear-thinning behavior over wide ranges of shear rates.

### 4.4.3 The Bingham Plastic Model

This model is the simplest mathematical expression describing the viscoelastic flow behavior. It is written as:

$$\tau_{yx} = \tau_0^B + \mu(\dot{\gamma}_{yx}) \quad for \quad \left| \tau_{yx} \right| > \left| \tau_0^B \right|$$
$$\dot{\gamma}_{yx} = 0 \qquad\qquad for \quad \left| \tau_{yx} \right| < \left| \tau_0^B \right| \tag{4.5}$$

### 4.4.4 The Herschel-Bulkley fluid model

The Herschel-Bulkley fluid is a simple generalization of the Bingham plastic model to cover the non-linear flow curve (for $|\tau_{yx}| > |\tau_0^B|$).

$$\tau_{yx} = \tau_0^H + \mu(\dot{\gamma}_{yx})^n \quad for \quad |\tau_{yx}| > |\tau_0^H|$$
$$\dot{\gamma}_{yx} = 0 \qquad\qquad for \quad |\tau_{yx}| < |\tau_0^H|$$

(4.6)

where $\tau_0$ is the yield stress.

This model satisfies better fit to experimental data with the use of three constants.

### 4.4.5 The Casson Fluid model

This model is derived for viscoeslatic fluid, and often used to describe biological fluids. The model has form as:

$$\left(|\tau_{yx}|\right)^{1/2} = \left(|\tau_0^c|\right)^{1/2} + \left(\mu|\dot{\gamma}_{yx}|\right)^{1/2} \quad for \quad |\tau_{yx}| > |\tau_0^c|$$
$$\dot{\gamma}_{yx} = 0 \qquad\qquad\qquad for \quad |\tau_{yx}| < |\tau_0^c|$$

(4.7)

where $\tau_0$ is the yield stress.

## 5. THE GOVERNING EQUATIONS

### 5.1 The Continuity Equation

In an infinitesimally fixed control volume in Figure 4.1, the rate of change of density is equal to the mass that flow into the element minus the mass that flows out the element. The equation of continuity is as following

$$\nabla \cdot \mathbf{V} = 0 \tag{5.1}$$

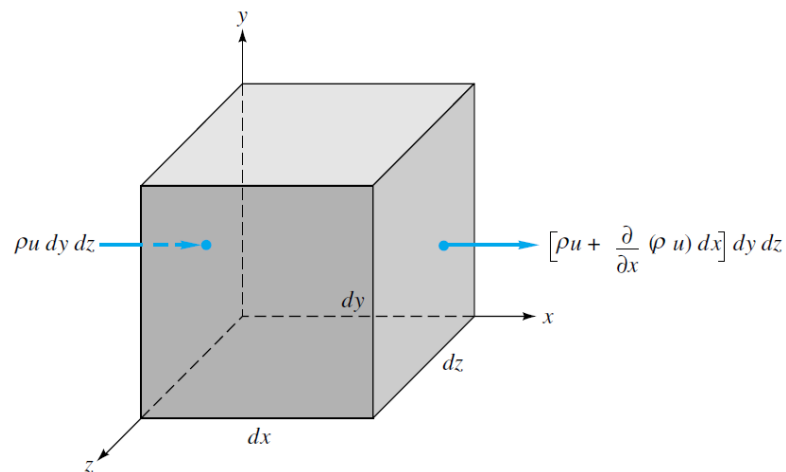**Figure 5.1 :** The control volume of fluid

### 5.2 The Momentum Equations

Applying the Newton's second law to the element of fluid, it can be said that the net force on the element of fluid is equal to the product of the density of fluid with the acceleration of the fluid. The net force on the element of the fluid is the surface forces which are due to the stresses on the sides of the element surface. These stresses are the sum of hydrostatic pressure and viscous stress $\tau_{ij}$. The Figure 5.2 illustrates the stresses on the element of fluid.
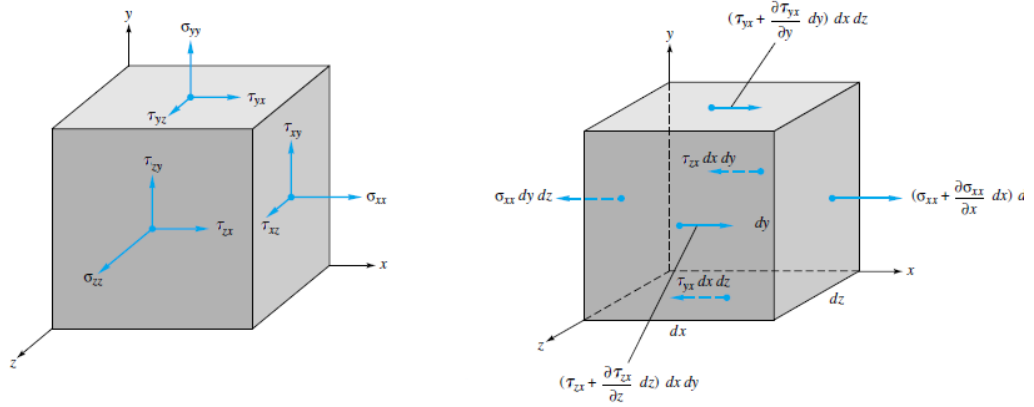
**Figure 5.2:** Stresses on the element of the fluid

The Newton second law on the element of fluid can be written for the element of fluid as following

$$-\nabla p + \nabla \cdot \boldsymbol{\tau} = \rho \frac{D\mathbf{V}}{Dt} \tag{5.2}$$

where $\mathbf{V}$ is the three-dimensional velocity vector, $t$ the time, $p$ the pressure, $\rho$ the density and $\tau$ the stress tensor. Writing the Navier-Stokes equations in this form allows the flexibility to use an arbitrary non-Newtonian blood viscosity model.

## 5.3 Linear Elastic Theory

In this study the structural behaviour of the vessel wall is represented as linear elastic material. The fundamental assumption of linear elasticity is small deformation. Therefore, in the case of small deformation, the first derivations of displacement vector which appears in the Green's strain tensor are very small, and the second derivation of displacement can be negligible. As a result of this, the Green's strain tensor reduce the form as following :

$$e_{ij} = \frac{1}{2}(\frac{\partial u_j}{\partial x_i} + \frac{\partial u_i}{\partial x_j}) \tag{5.3}$$

The Hooke's law constructs the relationship between the stress and the strain on a deformed body. For a three-dimensional state of stress, the generalized Hooke's law is:

22

$$\tau_{ij} = C_{ijkl} . e_{kl} \qquad\qquad\qquad\qquad (5.4)$$

where $C_{ijkl}$ is the tensor of elastic constants representing the mechanicals properties of material. In general form the Hooke's law has 36 $C_{ijkl}$ s. In rest state, $\tau_{ij} = \tau_{ji}$ because of the symmetry, so the number of $C_{ijkl}$ s reduce to 21. In addition to this, in the case of isotropic material the number of constant of $C_{ijkl}$ in the Hooke's law reduce to 2. The generalized Hooke's law then becomes:

$$\tau_{ij} = \lambda e_{xx} \delta_{ij} + 2\mu e_{ij} \qquad\qquad\qquad\qquad (5.5)$$

where $\lambda$ is Young's Modulus and $\mu$ is Poisson's ratio.

A linear relationship between stress and strain tensor exists in a material which is considered as linear elastic. Moreover, the stress at a point in the solid depends only on measure of strain at that point, and is independent of history of loading.

## 5.4 Boundary Conditions

At the input of the common carotid artery, Womersly velocity profile which fits the experimental flow data [21] which was obtained from a real artery bifurcation is used. In Figure 5.3 the inlet velocity profile, where its period is one second, is shown.
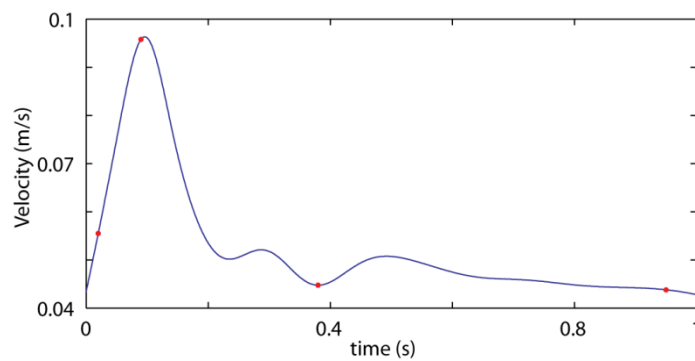


**Figure 5.3:** The Inlet Velocity Profile

23

The geometry of the common carotid artery is anatomically realistic, series of techniques are implemented to extract the actual artery from CT or MRI images of a patient using the Mimics Software [22, 23]. In the case of moving wall, the vessel wall is assumed as linear elastic material whose the scale of Young's Module is of order $10^5$ and the Poisson ration is in the range from 0.3 to 0.45. The density of blood is 1050 kg/m$^3$ .

## 6.  NUMERICAL METHODS

### 6.1 The Finite Volume Methods

In the present study, the finite volume method is used to discritize the geometric domain. In the finite volume method, the geometric domain is divided into number of control volumes such that there is one control volume surrounding each grid point. To obtain the numerical solution the differential equation is integrated over each control volume. Second-order upwind scheme is employed to compute the quantities at the faces. By this scheme higher-order accuracy is satisfied at the cell faces.

### 6.2 Pressure-Correction Methods

The pressure-correction method is used to achieve the numerical solutions. In the pressure-correction method, the iteration starts by guessing the pressure fields, p*. The values of p* are used to solve for velocity components, u, v and w from the momentum equation. The velocity components which solved in this step are denoted by u*, v* and w* due to the association with p*. These velocity components do not satisfy the continuity equation efficiently. The pressure correction, p', is constructed using the continuity equation. Summation of the pressure correction and p* gives the corrected pressure p.

$$p = p' + p* \qquad\qquad\qquad (6.1)$$

Similarly, the velocity components are corrected by adding the corrections, u', v' and w' to the velocity components of u*, v* and w*.

$$u = u' + u*$$
$$v = v' + v*$$
$$w = w' + w* \qquad\qquad\qquad (6.2)$$

These processes are repeated until a velocity fields are found that does satisfy the continuity equation.

## 6.3 Finite Elements Method

In the present study Finite Element Method (FEM) is used to obtain the numerical solution of the partial differential equations which describe the structure's behaviour. In this method, the structural system is modelled by a set of appropriate finite elements interconnected at points, called nodes. This method is based on getting the PDE into a system of linear equations and solving this system numerically using standard techniques.

## 6.4 Convergence Criteria

An iterative solution method requires a convergence and stopping criteria to terminate the iteration process. The measure of convergence is the change in the solution vector between successive iterations. The relative difference between consecutive solutions:

$$err = \frac{\left\| x^{(n+1)} - x^{(n)} \right\|}{\left\| x^{(n+1)} \right\|} \tag{6.3}$$

are used as the convergence criteria in the study. When the magnitude of the difference are less then $1 \times 10^{-3}$, the iteration will stop.

## 6.5 Validation of the Models

A reliable CFD model must satisfy several criterions, independent of time step size and independent of mesh size. To verify the validation of the model, the results obtained in different time steps, 0.1s, 0.01s and 0.001s are compared. Figure 6.1 shows the velocity distributions of these cases which same in qualitatively. However, small differences exist such as the maximum of the difference between 0.01s and 0.1s is 3.12% while the difference between 0.001s and 0.01s is 0.14%. So the model is independent of the time step size and we use 0.01s of step size in the calculations.
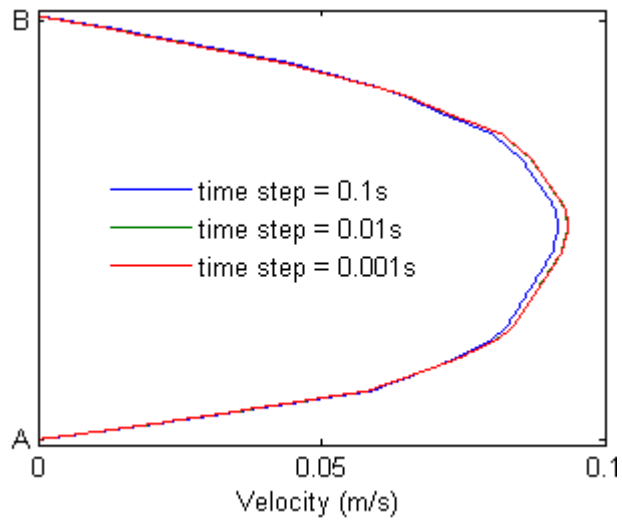
**Figure 6.1:** Velocity Profile of the Different Time Step Sizes

**Table 6.1:** Difference Mesh Sizes

|         | Number of Cells | Number of Faces | Number of Nodes |
|---------|-----------------|-----------------|-----------------|
| Size A  | 84159           | 180853          | 20928           |
| Size B  | 595301          | 1228065         | 118870          |
| Size C  | 872803          | 1796425         | 172045          |
| Size D  | 1302751         | 2668292         | 249603          |

Table 5.1 exhibits four distinct geometry cases with different mesh sizes. The Size A case has the coastest mesh while the Size D has the finest mesh.
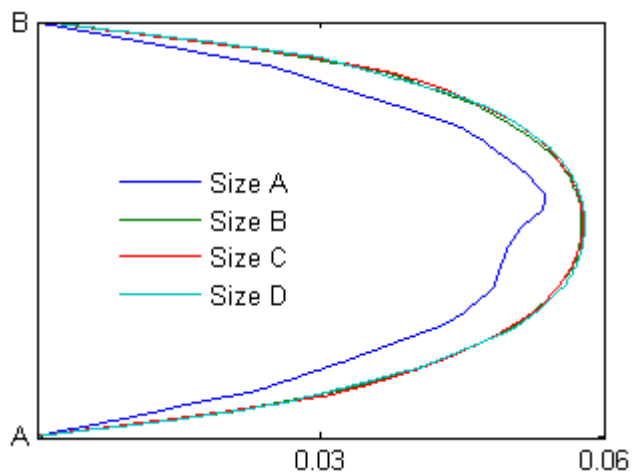


**Figure 6.2:** Velocity Profile of the Different Mesh Sizes

As it can be seen in Figure 5.2 the result of Size B, Size C and Size D are very close to each other. Moreover, the maximum difference occurs between Size B and Size C

and it is equal to 2.2%. However the results obtained using Size A gives smaller velocity distribution. The maximum difference between Size A and Size B is 20%. As a result, since the results of Size B, Size C and Size D are very close, using one of them in the simulation is convenient. In this study, simulation of all cases are done but only the results of Size C are represented in Result Section.

## 6.6 Fluid Structure Interaction

The blood flow simulation with moving boundary is studied in the present study. In the simulation, the behaviors of both fluid and solid wall must be considered and investigated. However, the physical properties of fluid and solid are distinct and can be described by different sets of differential equations, Navier-Stoke's Equations for fluid, and the Equilibrium Equation for the solid. Therefore, two separated systems constitute the blood flow simulation with moving boundary. The coupled system is illustrated in the Figure 5.3.
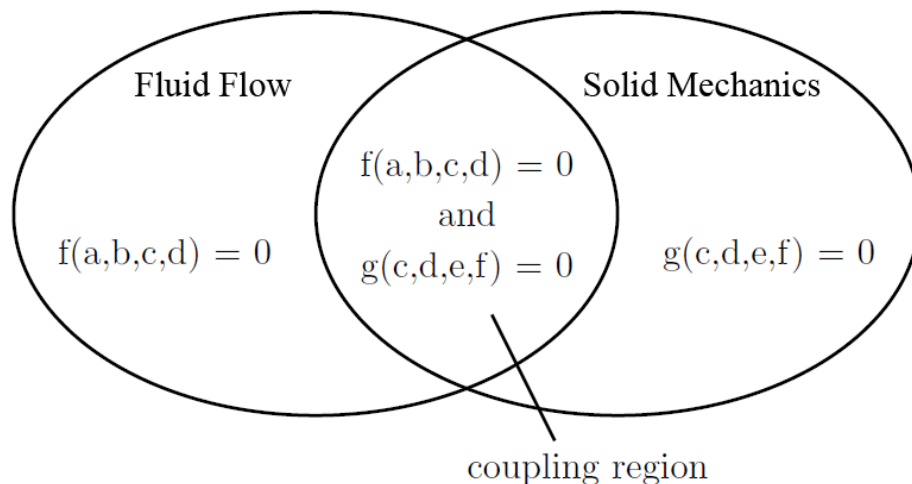


**Figure 6.3:** The Scheme of Coupled Systems

Although the two systems seem distinct to each other, they also share some variables. In the Figure 5.3, the coupling region contains the shared variables and coupling domain. In the blood flow simulation with moving boundary which is also called fluid structure interaction (FSI), the shared variables are pressure in fluid flow, and deformation in solid structure and the coupling domain is a 2D surface mesh.

The solution of FSI system requires appropriate data exchanges between fluid and solid code during the coupling process. The data exchange is a process that the data

is send and received from one solver to another solver. The data is defined on a mesh of the sender code and then shall be transferred to the mesh of the receiver code. These meshes present the same geometric entity, but differ in element size and node location, and this types of matching is also called as "non-matching grids" as shown in the Figure 6.4. The data exchange process consists of two steps, association and interpolation. In the association step, for each node or element of one mesh, the partners on the other mesh must be found. This process is also called neighborhood search. In the interpolation step, the data which shall be transfered must be adapted to the target mesh. The data will be exchanged between associated nodes by means of interpolation. After association step, if a node is not associated to an node of other grid then it is called "orphaned" elements and this node neither send nor receive any data.
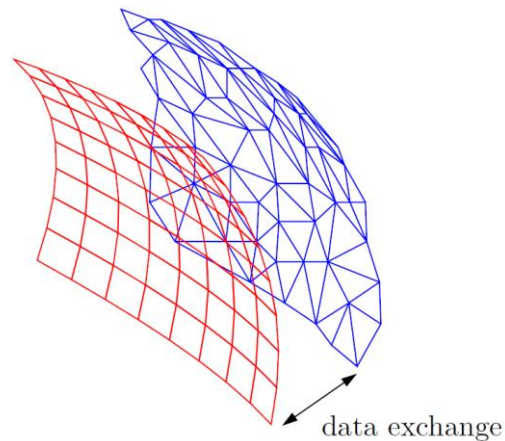


**Figure 6.4** Data exchange between fluid and structure

The coupling process consists of three main steps; initialization, iteration and finalization. In the initialization step, the codes initialize their data and the partner of each node are determined by executing the neighborhood search process. In the iteration step, each codes compute their part of the problem and data is exchanged at the certain time. During the iteration step, the data exchanged several times according to the coupling algorithm which consists of send- and/or receive- functions at different states of computation. Depending on the problem types the data can be exchanged:

- At the beginning of the each time step

- At the end of the each time step

- Before or after an iteration step

Each subsystem is solved separately and the pressure and displacement are exchanged and inserted into the equation of the other problem. The FSI simulation starts with solving the Navier-Stoke's equation and pressure values are calculated. While the Navier-Stoke's is being solved, the solid mechanics simulation waits for the pressure value to start the calculations. When the Navier-Stoke's is solved succesfully, the pressure data are sended from Fluid Flow Simulation to Solid Mechanics Simulation. After one succesful step and sending the pressure data, the Fluid Flow Simulation waits until the displacement data is received from Solid Mechanics Simulation.

Receiving the pressure data starts the calculation on the Solid Mechanics Simulation and the displacement data is obtained by this step. The resultant displacement data are sended to the Fluid Flow Simulation which waits for the data. The processes described above, is illustrated in the Figure 6.5.
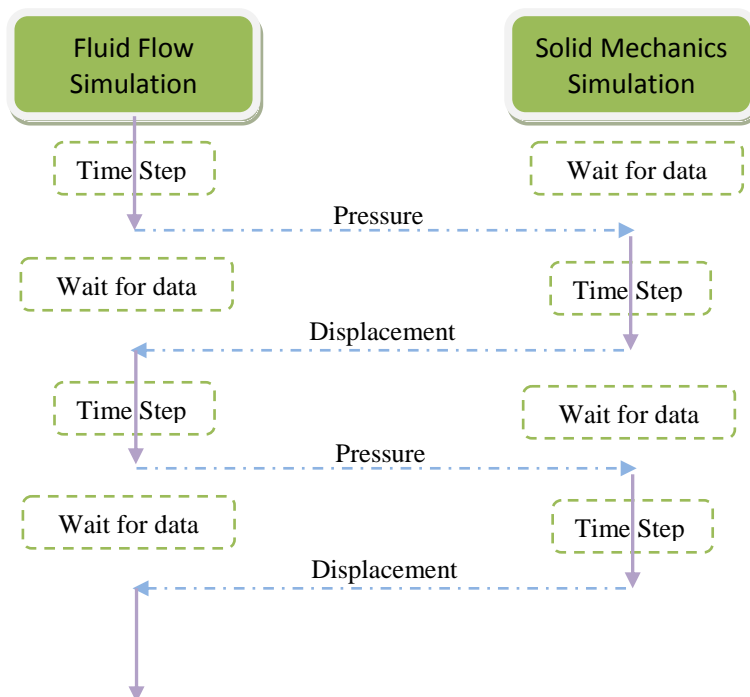
**Figure 6.5:** The Process of FSI

## 6.7 Construction of the Geometric Domain

The geometric model which used in this study has been constructed from human CT images. The CT images are shown by 3 distinct planes: axial, coronal and saggital in the Figure 6.6. The construction process consists of number of steps. The first step is defining the vessel on the images by adjusting the Hounsfield scale. The Figure 6.7 shows a slice on which the Hounsfield scale is applied with proper range for vessel. The tissues which are in same range of Hounsfield scale may also be marked in this step. One more step for clearing up these tissues is necessary. Deleting the undesired tissues from the mask on the slice completes the defining vessels process. When the clearing up process is achieved the mask contains only the vessels. To complete defining process on whole domain successfully, these steps are applied all CT slices.

After the defining process is completed successfully, 3D representation of the mask is constructed as shown in the Figure 6.8. The 3D representation is a surface mesh which consists of triangles. The surface mesh is generated by way of interpolation on the vessel contours. After number of smoothing process on the 3D surface mesh, this step is completed successfully.

A last step is required to fill the interior of domain with unstructured tetrahedral elements. Once the last step is achieved the geometric domain is ready to CFD analysis.

The processes of defining vessel mask and construct 3D surface mesh are implemented with MIMICS which is a commercial software. The last step is applied with TGRID which a commercial software.
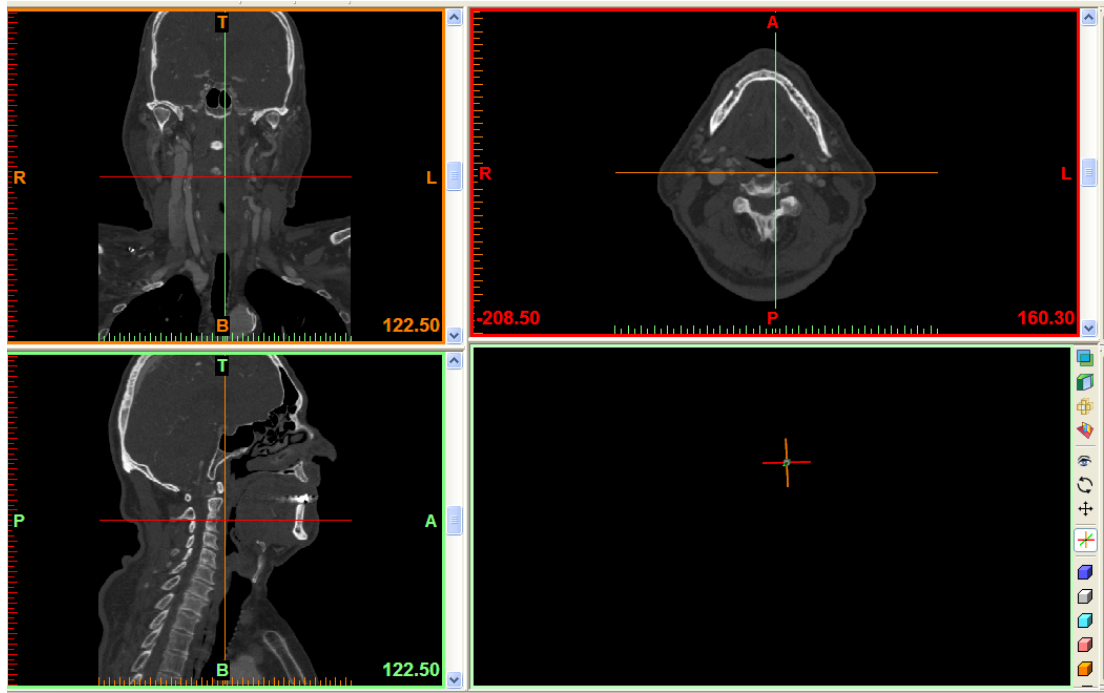
**Figure 6.6 :** The CT images
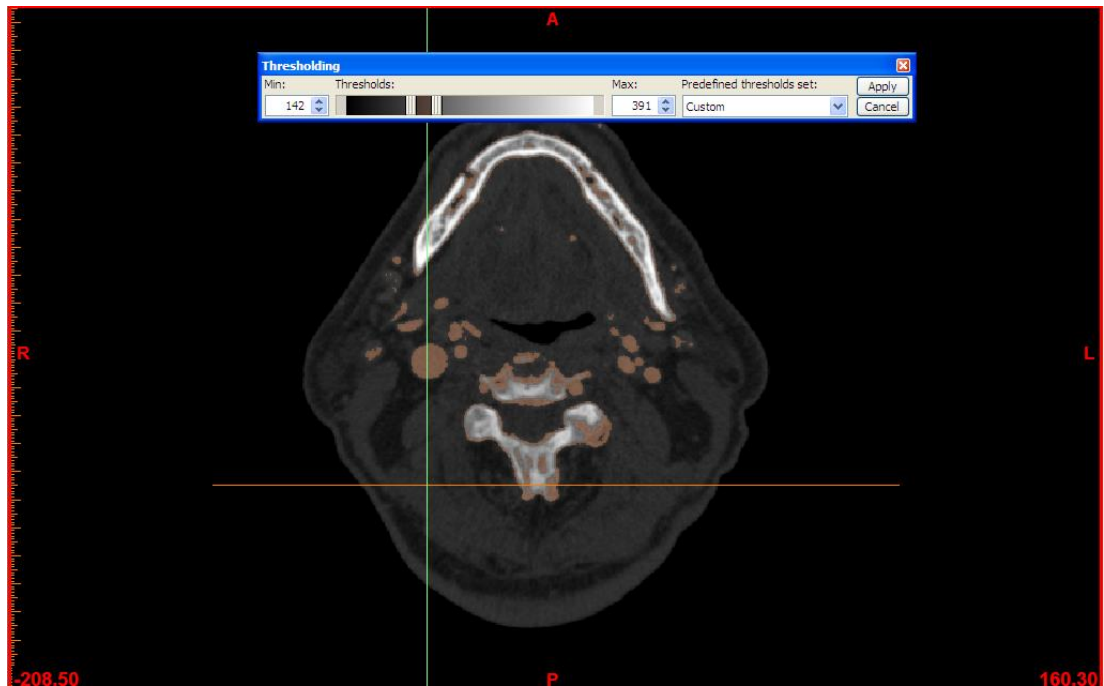


**Figure 6.7 :** The slice on which Hounsfield scale is applied

**Figure 6.8 :** 3D representation of arterial vessel

# 7. RESULTS

In this section, to investigate the effect of non-Newtonian models, simulation results of all viscosity models are compared. On three distinct regions WSS distributions are compared for four time-steps on unsteady flow with rigid wall assumption. One of the regions is the Carotid Sinus on where a lot of diseases occur. The WSS distribution on this region is responsible the occurrence of the many disorders. Another region is the carotid bifurcation. Because the blood flow is forced for separation (stagnation point), very high velocity gradient exists on this region. The third region is a region on common carotid before the bifurcation. On this region there is not any stenosis or dilatation, and the curvature on this region is very low therefore the velocity gradient is very small. The comparisons on this region are made because of the small velocity gradient on this region.

Moreover, the velocity profiles of each cases are investigated along 3 lines inside the artery. These three lines are located before the carotid bifurcation, on carotid bifurcation, and the carotid sinus.

And finally, the results of simulations with the assumption of rigid wall and moving wall are compared. The effect of the assumption of rigid wall with non-Newtonian fluid is analysed by comparing the results of rigid wall and moving wall. Moreover, to assess the effects of non-Newtonian viscosity, the comparison of WSS distributions of different viscosity models are made in three regions.

## 7.1 Main Carotid Bifurcation
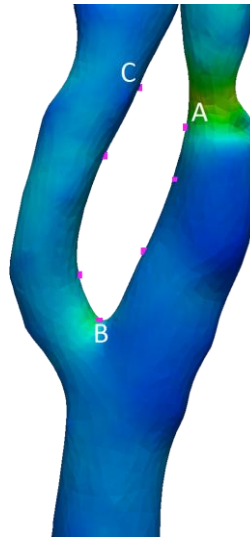


**Figure 7.1:** Main bifurcation of the Carotid artery
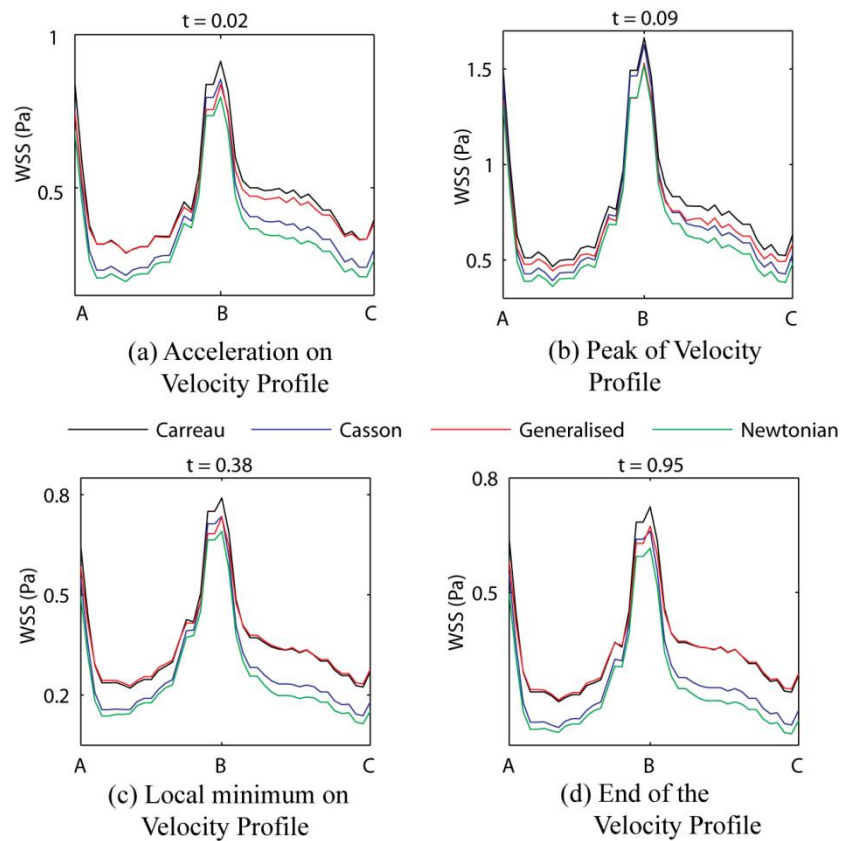


**Figure 7.2:** WSS distributions of various viscosity models

The flow is forced for separation on main bifurcation of the carotid artery. This region has very high velocity gradient due to the separation. In Figure 7.2, the WSS

distributions of different viscosity models at different time steps are presented. On the main bifurcation of carotid artery, the maximum WSS occurs on the stagnation point because of the high velocity gradient. Moreover, the relative differences with non-Newtonian and Newtonian models are minimum on this point due to the high shear rates. On the stagnation point, the Carreau model gives the highest WSS values at all time steps. In this region, Generalised Power Method and Carreau models have very close results. However, on the stagnation point, the difference between the results of Carraeu and Generalised Power models is increased significantly. Furthermore, the Casson model causes WSS distribution that is similar to the Newtonian model. The difference between the Casson and Newtonian models is increased on the stagnation point but the rate of difference is remained unchanged.

**Table 7.1:** Differences between the results of non-Newtonian models and Newtonian model

| | Newtonian | | | | | |
|---|---|---|---|---|---|---|
| | Maximum | | Minimum | | Mean | |
| Carreau | 58.7% | 0.159 Pa | 13.9% | 0.058 Pa | 38% | 0.095 Pa |
| Generalised Power Method | 58.6% | 0.13 Pa | 2.7% | 0.02 Pa | 33% | 0.12 Pa |
| Casson | 14.9% | 0.07 Pa | 5.8% | 0.02 Pa | 10% | 0.04 Pa |

Table 7.1 shows the maximum, minimum and mean value of the difference and the relative difference. The values in the Table 7.1 is calculated from simulations at t=0.02 sec. of period. From Table 7.1, it can be seen that, despite of small quantitative difference in WSS, the rates of difference which are up to 59% are significant,
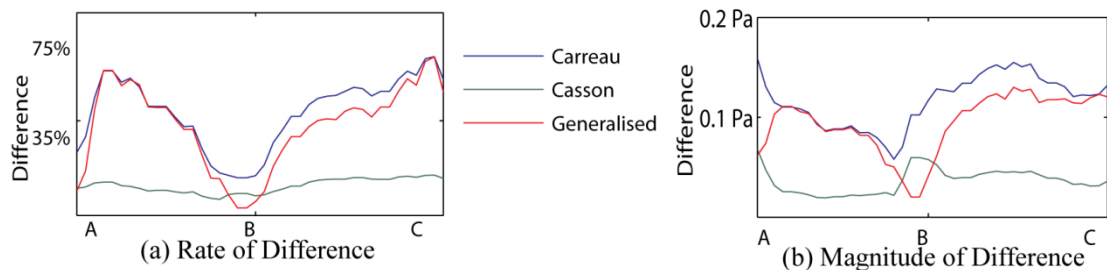


**Figure 7.3 :** Difference rate and magnitude of WSS distributions

Figure 7.3 shows the differences and the rates of difference at the path which span from A to C. The rate of difference is the minimum at the stagnation point because of high strain rates. Moreover, the Generalised Power Method gives closer results to that of Newtonian model at the high shear rates. The rate of difference between the Casson model and Newtonian has same the tendency along the path from A to C.

## 7.2 Carotid Sinus

The sinus region of internal carotid is one of the most problematic region. Accumulation of plaque occurs on this region due to the high WSS distribution. At the sinus region of internal carotid artery, WSS increases as the artery gets narrower and reaches its biggest effect at the narrowest zone. The difference between non-Newtonian and Newtonian effects is the minimum in this zone which has the maximum WSS. While the artery enlarges after the narrowest region, the value of WSS decreases rapidly. On the other hand, the difference between non-Newtonian and Newtonian effects increases rapidly. The Carreau and Generalised Power Method generally give similar WSS distribution, but at the peak point of WSS, the results of Generalised Power Method move away from the results of Carreau and get close to the results of Newtonian. The Casson model is a non-Newtonian model which generally results lowest WSS values. However, on the peak values of WSS, the Generalised Power Method gives lower values than that of the Casson. Moreover, the Casson and the Newtonian model results show that the rate of difference in WSS distribution is not significantly change in the region spanning from A to B.
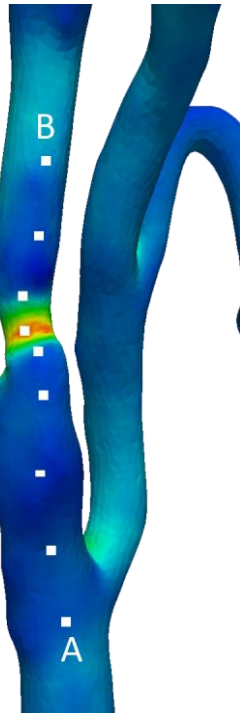
**Figure 7.4 :** Carotid Sinus
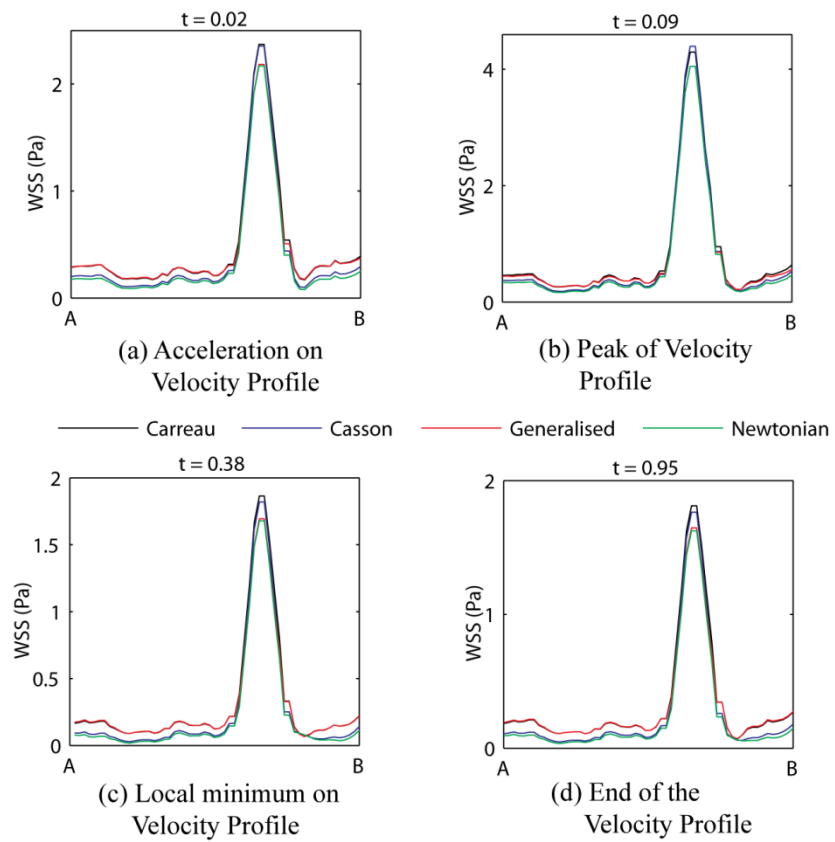


**Figure 7.5 :** WSS distributions of various viscosity models

**Table 7.2:** Differences between the results of non-Newtonian models and Newtonian model

| | Newtonian | | | | | |
|---|---|---|---|---|---|---|
| | Maximum | | Minimum | | Mean | |
| Carreau | 123.5% | 0.203 Pa | 9.3% | 0.07 Pa | 60.6% | 0.12 Pa |
| Generalised Power Method | 130.1% | 0.142 Pa | 0.4% | 0.006 Pa | 60.2% | 0.09 Pa |
| Casson | 26% | 0.185 Pa | 8.5% | 0.02 Pa | 15.15% | 0.04 Pa |

Table 7.2 shows that the Generalised Power Method has the maximum and the minimum rate of difference. At the Carotid Sinus the rate of difference is up to 130%. The mean and maximum value of rate of difference of Carreau and Generalised Power Method are close.
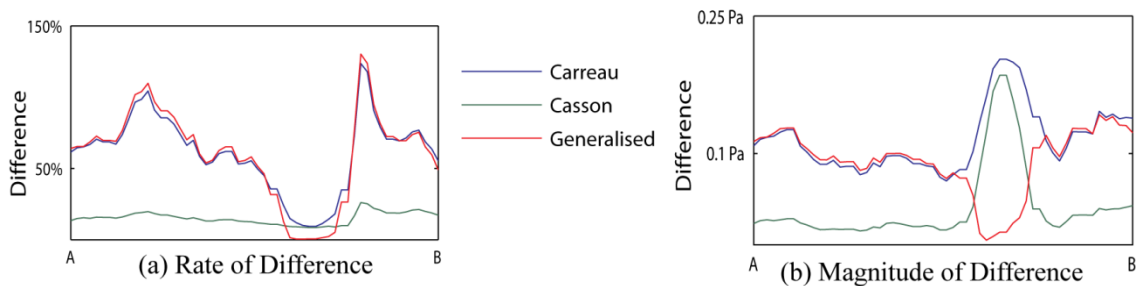


**Figure 7.6 :** Difference rate and magnitude of WSS distributions

The rate and magnitude of difference along the path spanning from A to B are shown in the Figure 7.6. The Carreau and Generalised Power Method have the same tendency in the rate of difference, but the magnitude of difference of these two models differs on the point which has the maximum WSS. While the difference between Carreau and Newtonian increases, the difference between Generalised Power Method and Newtonian decreases at that point.

## 7.3 Common Carotid
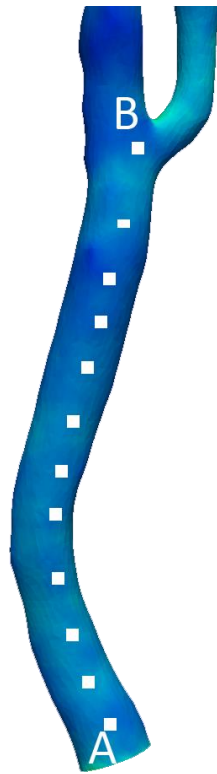


**Figure 7.7 :**Common Carotid



(a) Acceleration on
Velocity Profile

(b) Peak of Velocity
Profile

Carreau ——— Casson ——— Generalised ——— Newtonian

(c) Local minimum on
Velocity Profile

(d) End of the
Velocity Profile
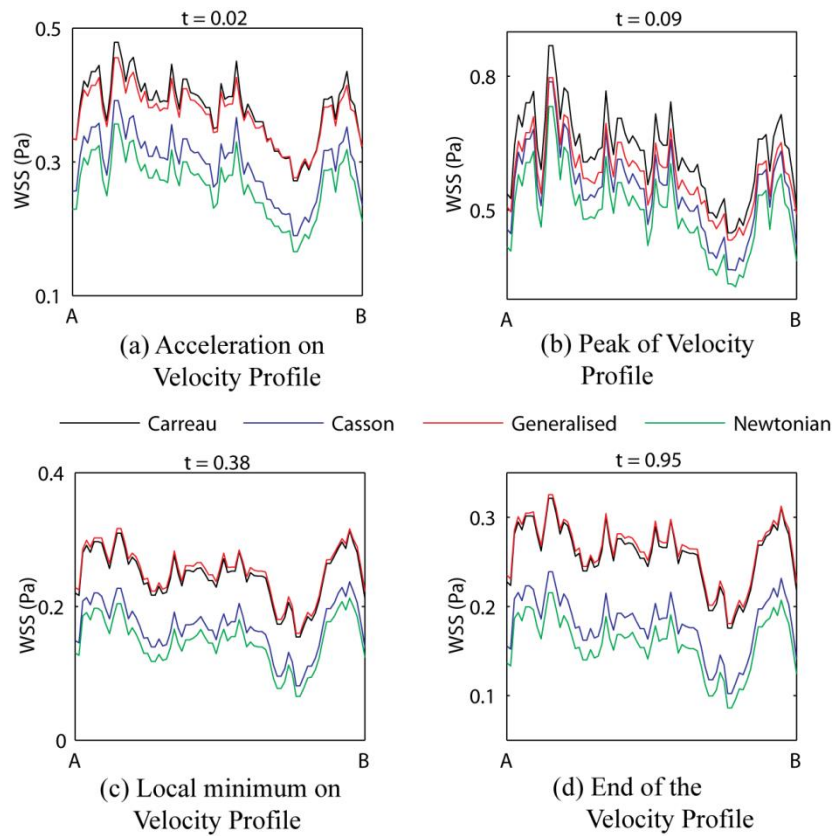
**Figure 7.8 :** WSS distributions of various viscosity models

Since the radius in the Common Carotid artery does not change very much and the artery has not any significant increase on curvature, the WSS distribution along the artery does not exhibit a big change. On the path spanning from A to B, the Carreau and Generalised Power Methods give higher WSS distribution than that of Newtonian. Furthermore, the differences of both Carreau and Generalised Power Method with Newtonian model are small. The Casson model gives the lowest WSS distribution in this region. At the highest inlet velocity (see Figure 7.8.b ), the WSS distribution of each model gives closer results which are an expected behavior of the non-Newtonian models.

**Table 7.3:** Differences between the results of non-Newtonian models and Newtonian model

|  | Newtonian | | | | | |
|  | Maximum | | Minimum | | Mean | |
|---|---|---|---|---|---|---|
| Carreau | 63.9% | 0.128 Pa | 34.3% | 0.103 Pa | 44.5% | 0.116 Pa |
| Generalised Power Method | 66.7% | 0.122 Pa | 27.7% | 0.093 Pa | 41.3% | 0.106 Pa |
| Casson | 14.6% | 0.038 Pa | 9.8% | 0.02 Pa | 11.8% | 0.031 Pa |

Table 7.3 shows the value of rate of difference and the magnitude of difference at the Common Carotid. Although the Generalised Power Method has the maximum rate of difference, the biggest mean rate of difference is belong to Carreau. The smallest rate of difference occurs between Casson and Newtonian.
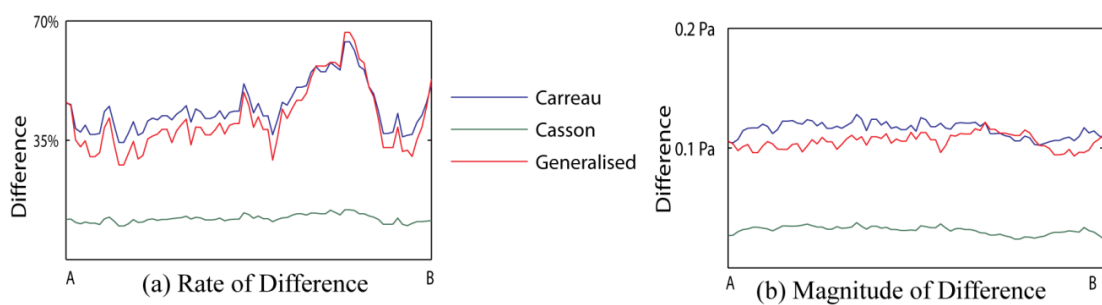


**Figure 7.9 :** Difference rate and magnitude of WSS distributions

Figure 7.8 shows that, despite the fact that the magnitudes of differences along the path spanning from A to B have not significant changes, the rates of differences have big changes (see Figure 7.9.a) except the Casson model.

## 7.4 Velocity Profiles of Main Bifurcation
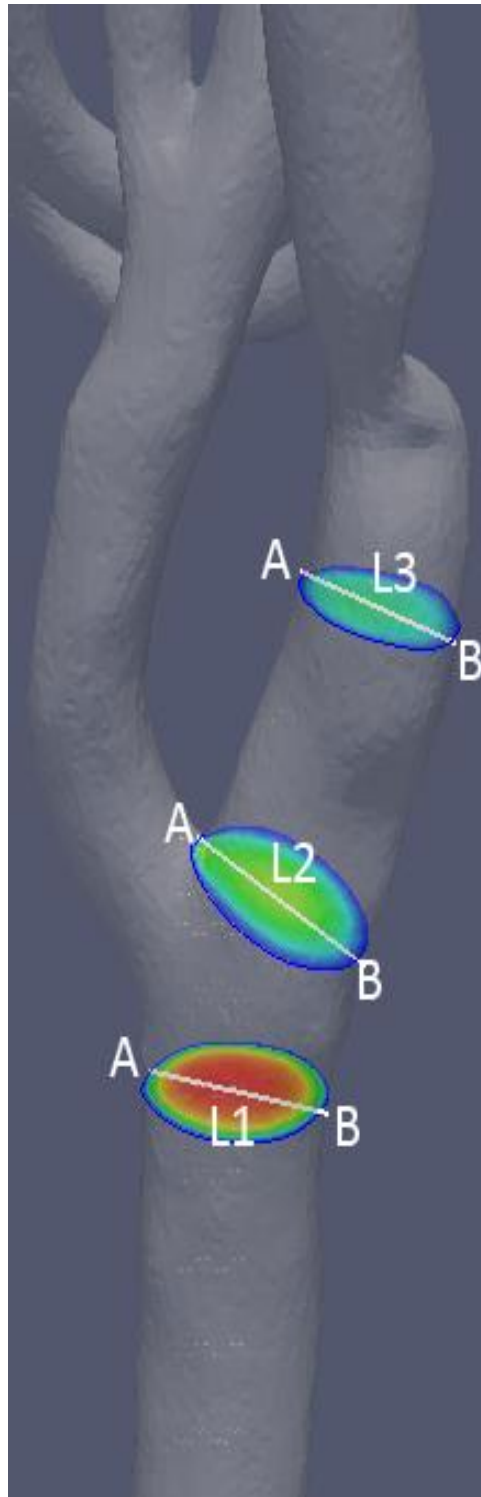


**Figure 7.10 :**Lines
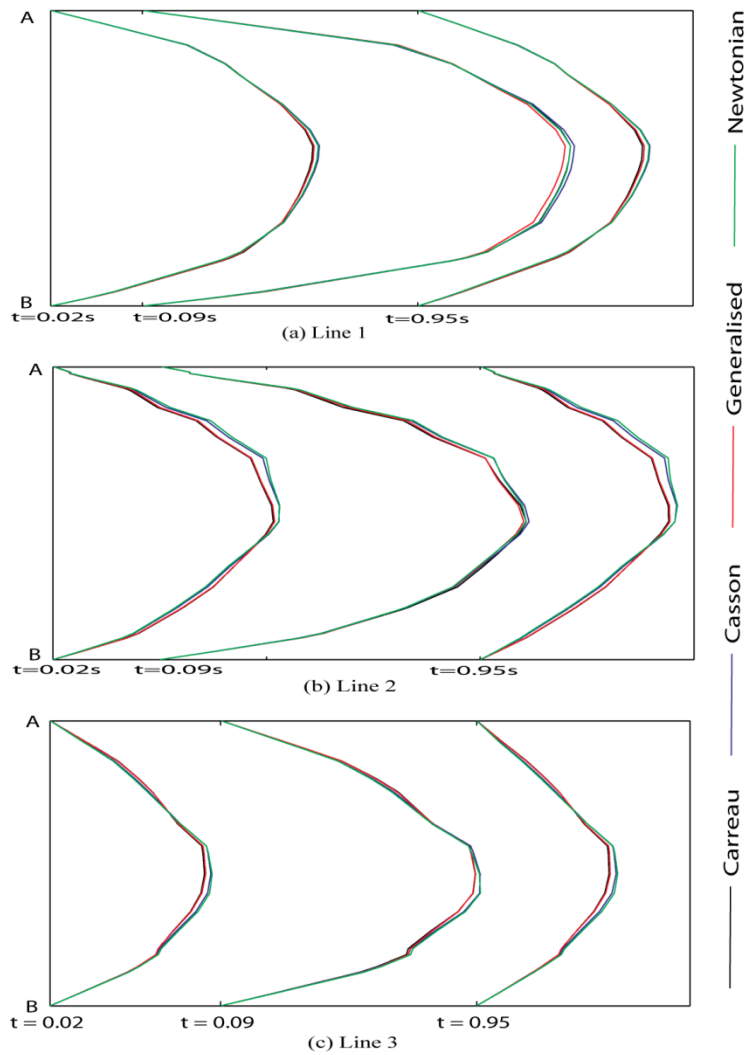
**Figure 7.11 :** Velocity profiles of various viscosity models

In this section the effects of non-Newtonian properties on velocity profiles are discussed. To assess this effect, the velocity profiles along three lines inside the arteries are compared.

Velocity profiles of non-Newtonian and Newtonian model simulations are studied on three distinct lines inside the arteries. The first of these lines, L1, is located right before the main bifurcation, the second line, L2, is on both the main bifurcation and entrance of internal carotid artery, and the last line, L3, is located on the largest zone of the carotid sinus (see Figure 7.10).

Due to the lower shear rate on the centre-line of the artery, the non-Newtonian properties are dominant in this region. Because, the shear rate near the artery walls is higher, the impact of non-Newtonian effects is not dominant on velocity profiles on this region. As it can be seen in the Figure 7.11, while the velocity profile of a

Newtonian model is paraboloid, the non-Newtonian models cause flatter velocity profiles according to shear-thinning properties of non-Newtonian models. Furthermore, the differences between non-Newtonian and Newtonian models are greater in the centre-line. Generally the Carreau and the Generalised Power Methods are in the same tendency.

The comparison of the velocity profiles on L1, L2 and L3 lines indicates that the bigger velocity gradient from A to B results an increment of non-Newtonian properties. In L1 line, the velocity gradient is smaller and velocity profile is smoother then the values of difference rate under 5%. Moreover, in the L2 line, the value of difference rate is about 20% because of the higher velocity gradient and the rougher velocity profile. Figure 7.12 shows the differences and the differences rate with non-Newtonian and Newtonian models.
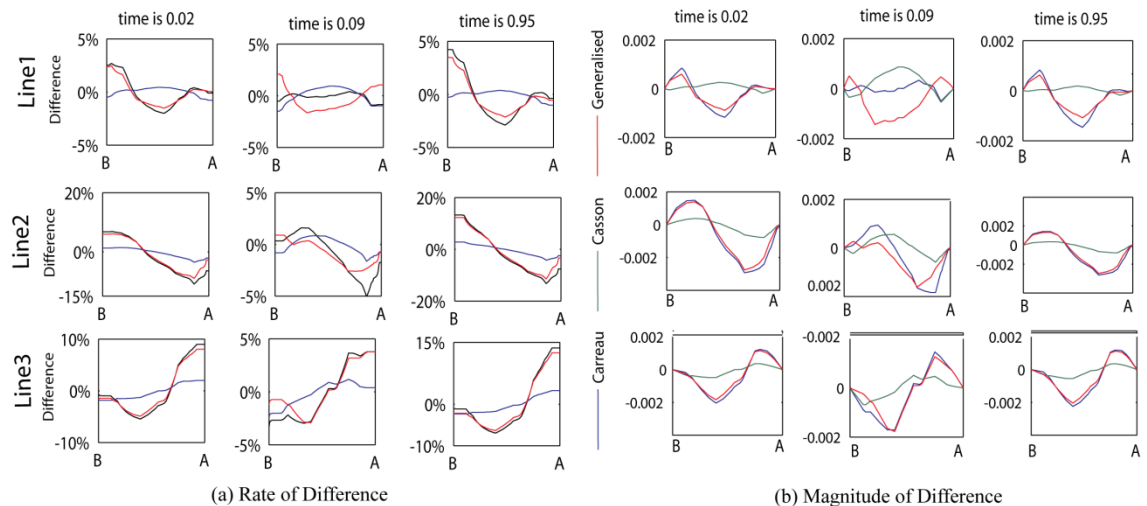


**Figure 7.12 :** Differences between non-Newtonian and Newtonian on Velocity Profiles

## 7.5 Blood Flow and Moving Vessel Wall Interaction

To investigate the effect of the moving wall on the WSS distributions, the comparison of results of moving boundary and rigid boundary is made. In the simulations Carreau, Casson and Generalised Power Method viscosity models are used to incorporate the blood rheology. As it can be seen in figures, moving boundary results in higher WSS distribution. The difference between the moving and rigid boundaries increases when the velocity gradients are higher. At the time of 0.09s the velocity inlet profile has maximum value and at the time of 0.38s the

velocity inlet profile has the minimum value. Therefore, the difference between the WSS distribution at t=0.09s and the WSS distribution at t =0.38s occurs due to the velocity magnitude at these time steps.

### 7.5.1 Rigid-Moving Wall Comparison of the Casson viscosity
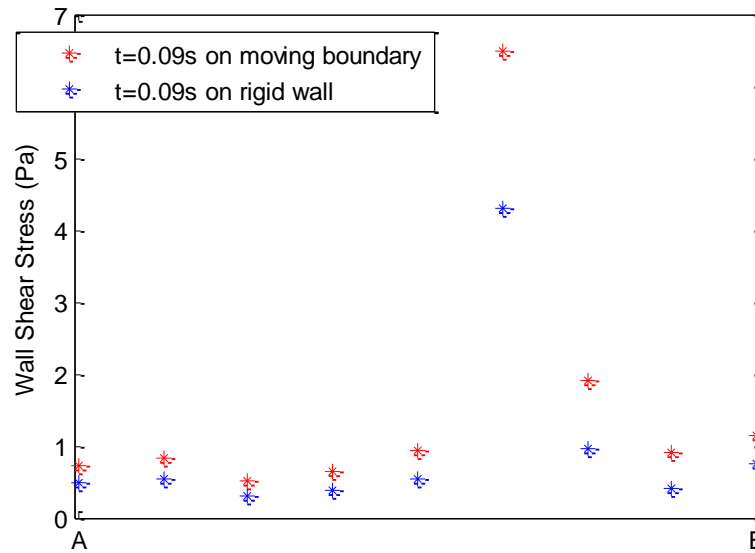


**Figure 7.13 :** On A region, WSS differences between moving boundary and rigid wall at time 0.09s
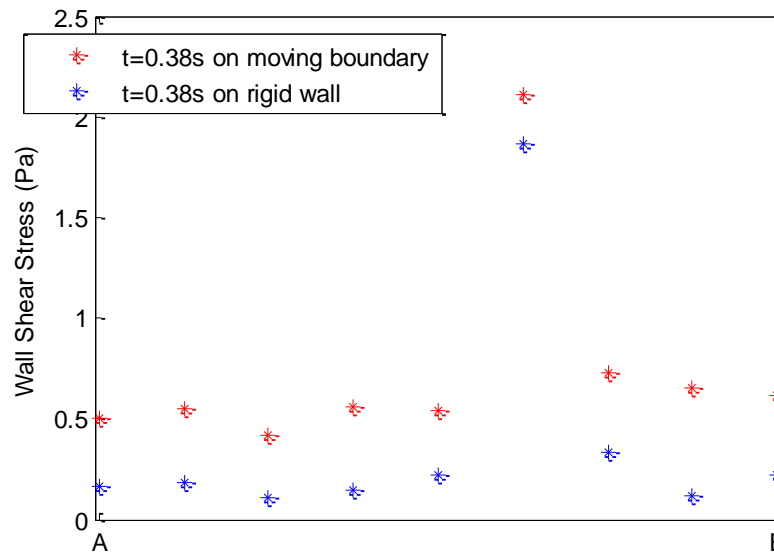


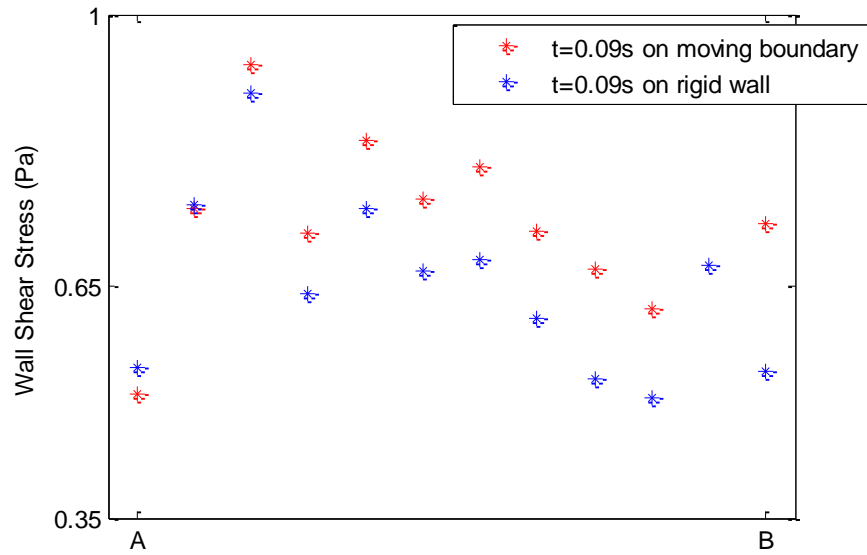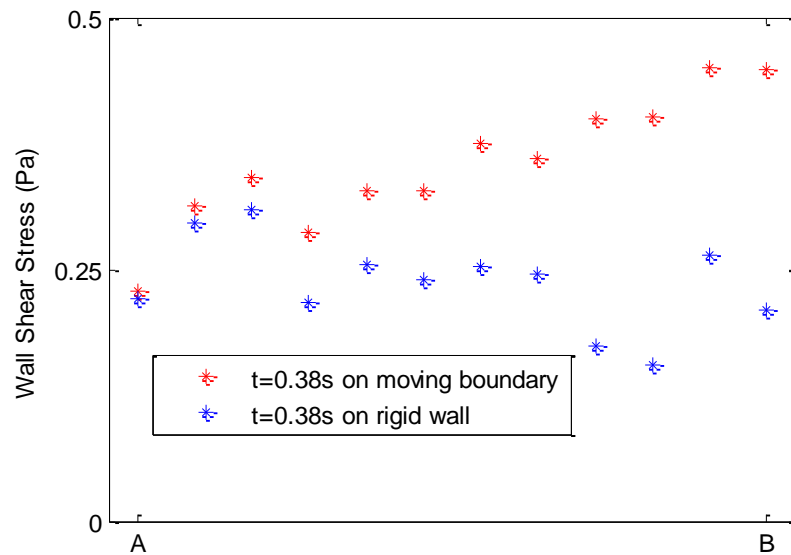**Figure 7.14 :** On A region, WSS differences between moving boundary and rigid wall at time 0.38s

**Figure 7.15 :** On C Region, WSS differences between moving boundary and rigid wall at time 0.09s



**Figure 7.16 :** On C Region, WSS differences between moving boundary and rigid wall at time 0.38s

**7.5.2 Rigid-Moving Wall Comparison of Generalised Power Method viscosity**
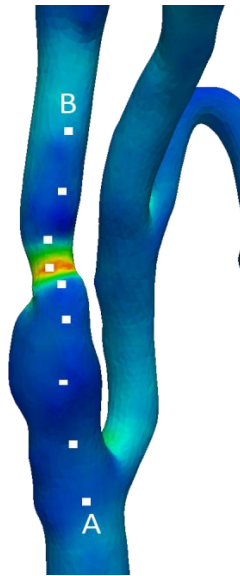


**Figure 7.17 :**Carotid Sinus
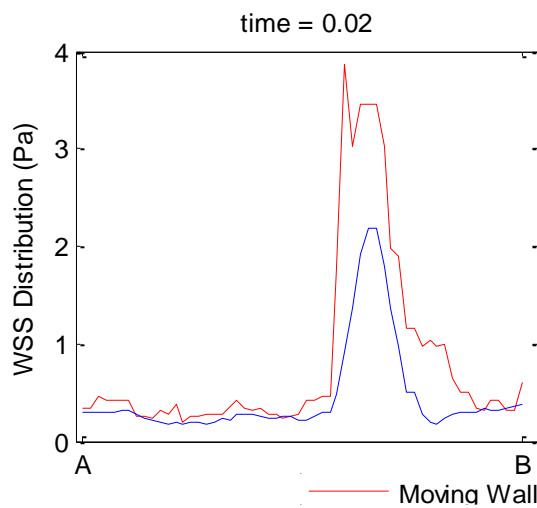


**Figure 7.18.a :**Difference at time=0.02s     **Figure 7.18.b :**Difference at time=0.09s
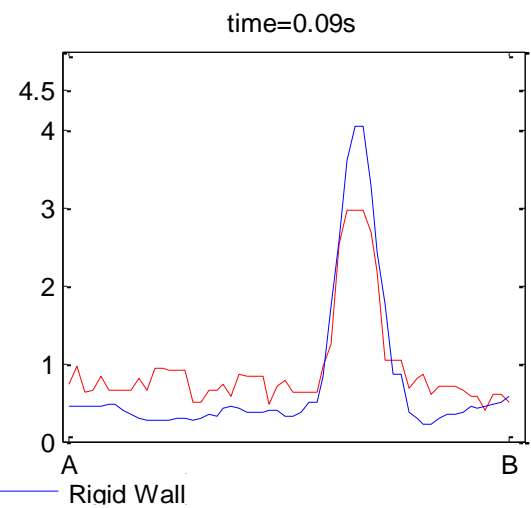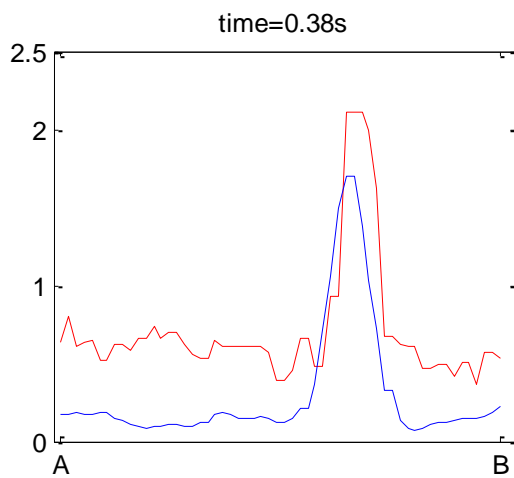


**Figure 7.18.c** :Difference at time=0.38s     **Figure 7.18.d** :Difference at time=0.95s
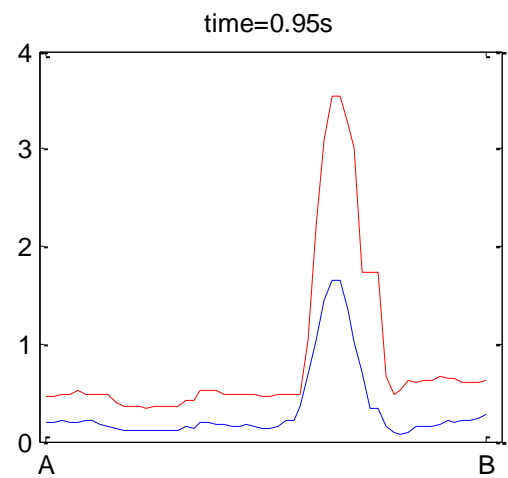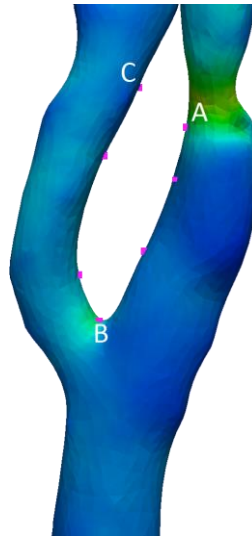
**Figure 7.19:** Main bifurcation of the Carotid artery
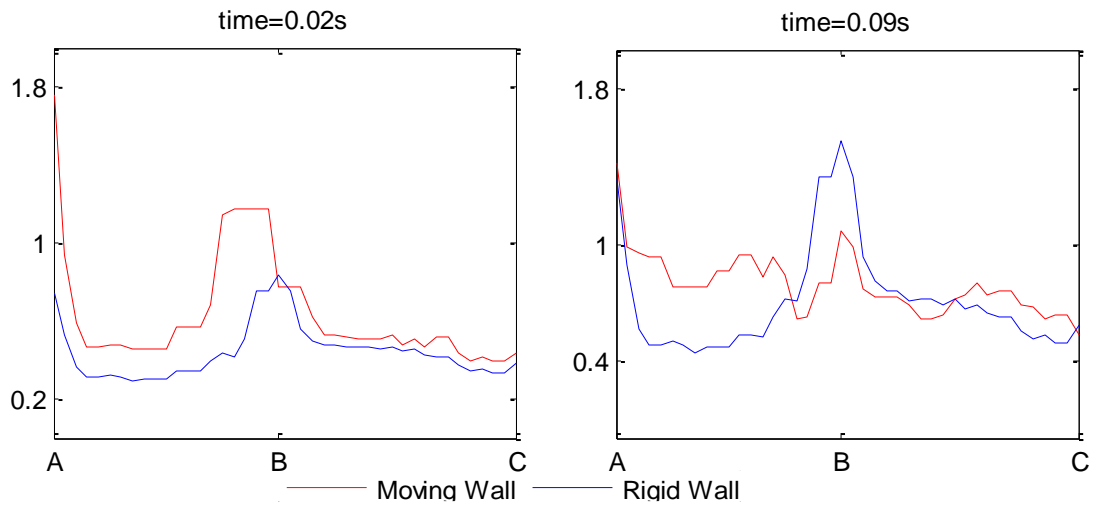


**Figure 7.20.a :**Difference at time=0.02s    **Figure 7.20.b :**Difference at time=0.09s
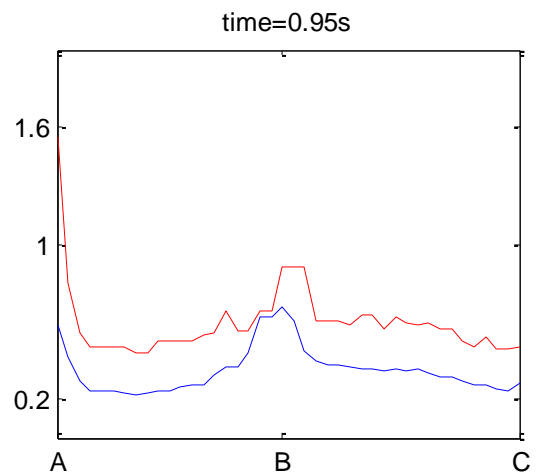


**Figure 7.20.d** :Difference at time=0.95s
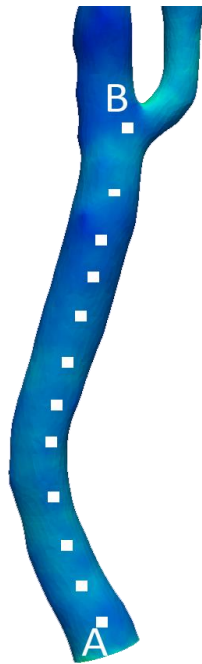
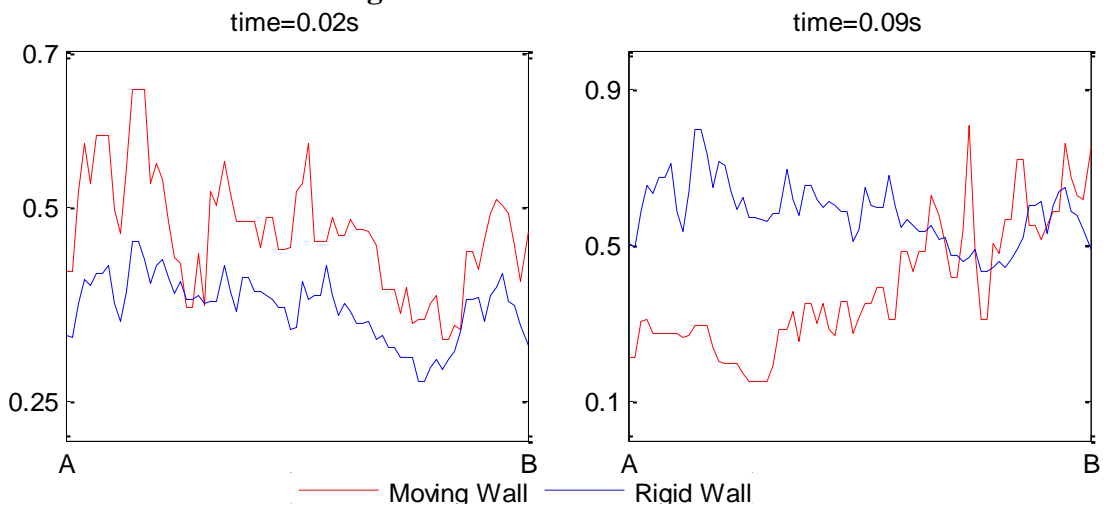**Figure 7.21:** Common Carotid



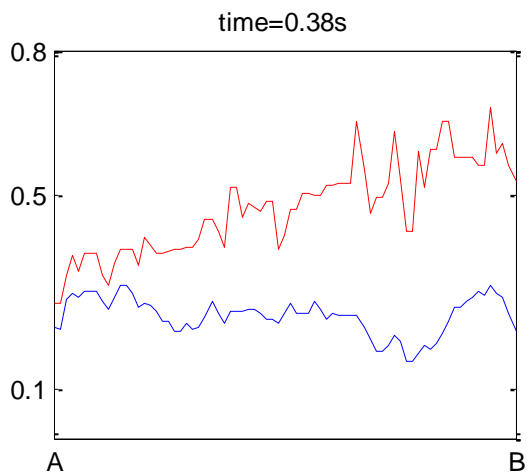**Figure 7.22.a :**Difference at time=0.02s   **Figure 7.22.b :**Difference at time=0.09s



**Figure 7.22.c** :Difference at time=0.38s
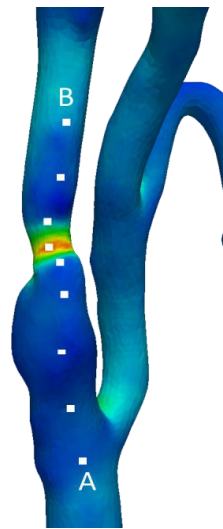
### 7.5.3 Rigid-Moving Wall Comparison of Casson viscosity
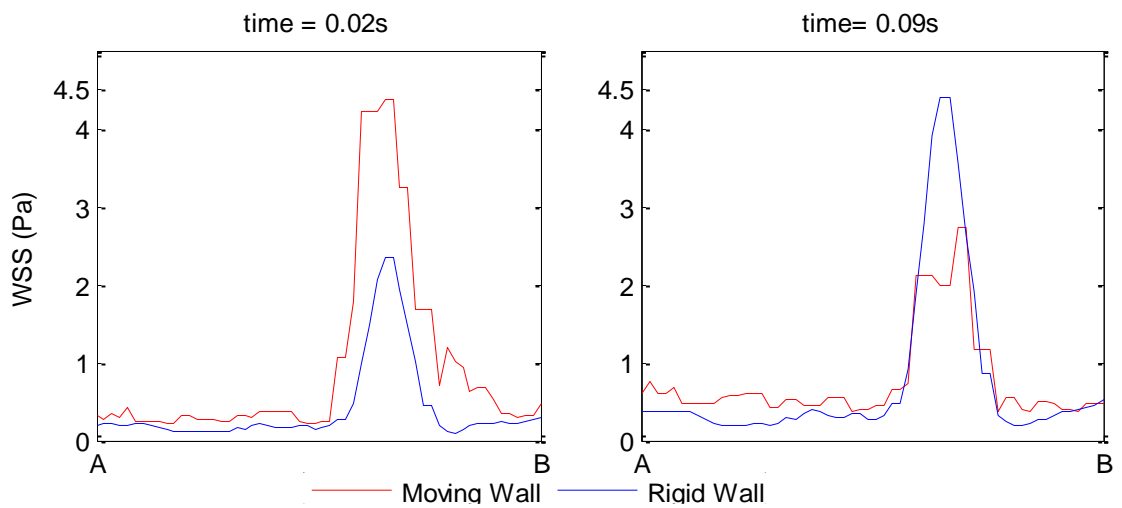


**Figure 7.23 :**Carotid Sinus



**Figure 7.24.a :**Difference at time=0.02s     **Figure 7.24.b :**Difference at time=0.09s
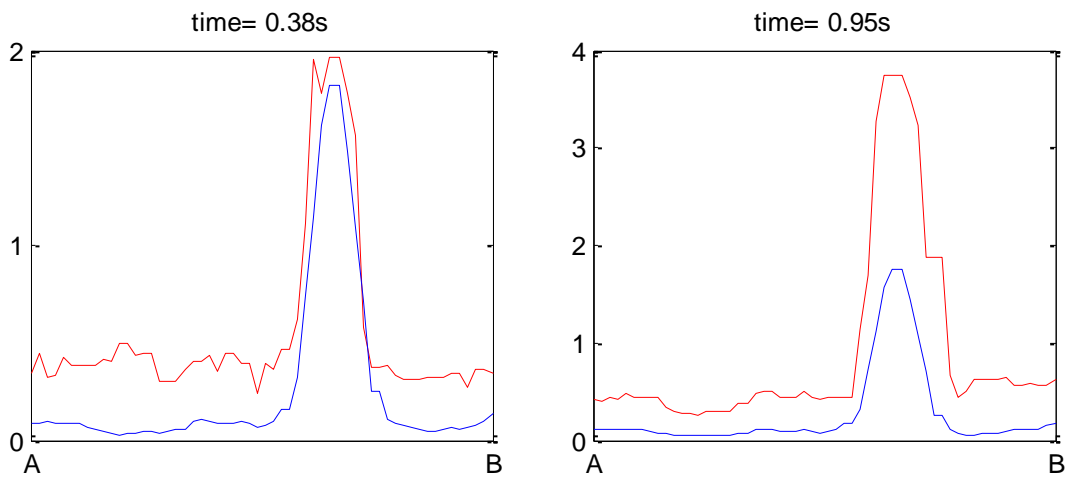


**Figure 7.24.c** :Difference at time=0.38s     **Figure 7.24.d** :Difference at time=0.95s
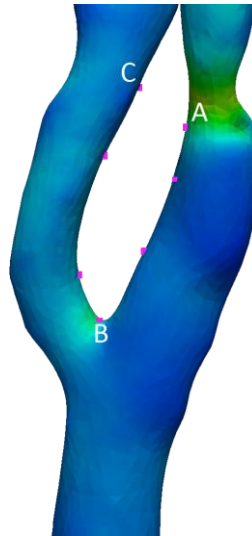
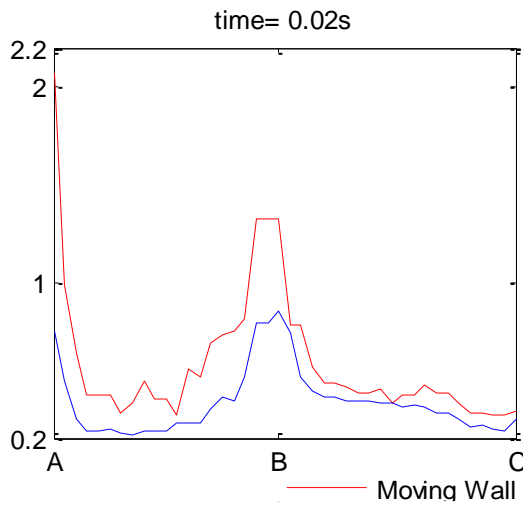**Figure 7.25:** Main bifurcation of the Carotid artery



**Figure 7.26.a :** Difference at time=0.02s    **Figure 7.26.b :** Difference at time=0.09s
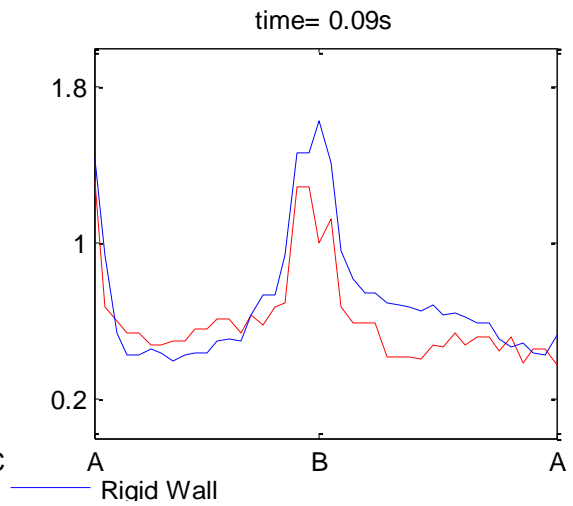


**Figure 7.26.c :** Difference at time=0.38s    **Figure 7.26.d :** Difference at time=0.95s
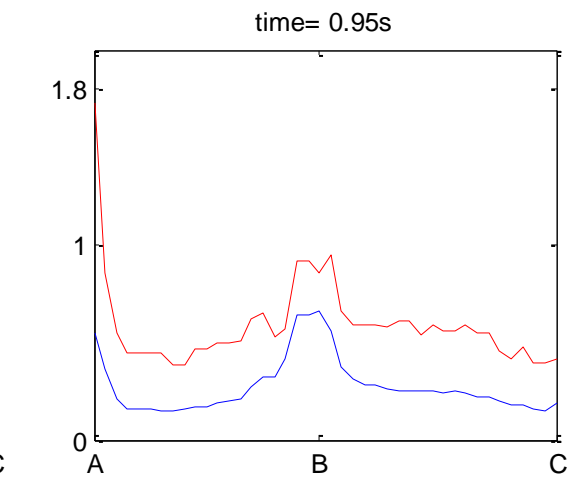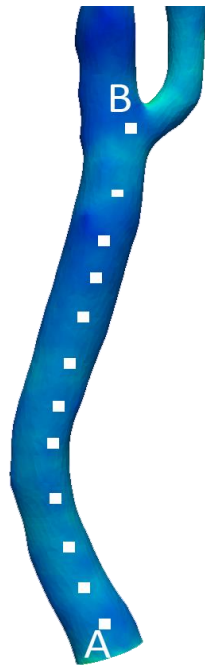
**Figure 7.27:** Common Carotid



time= 0.02s



time= 0.09s

Moving Wall ——— Rigid Wall

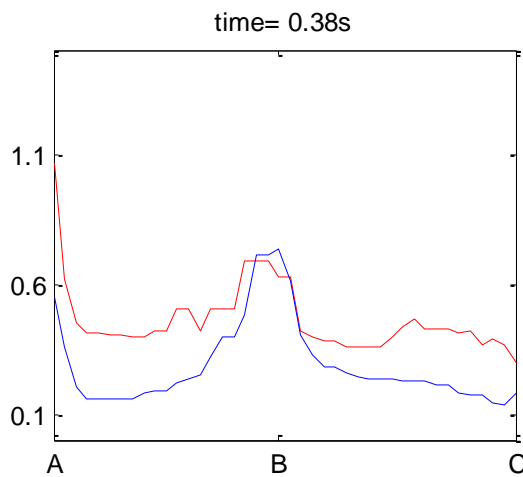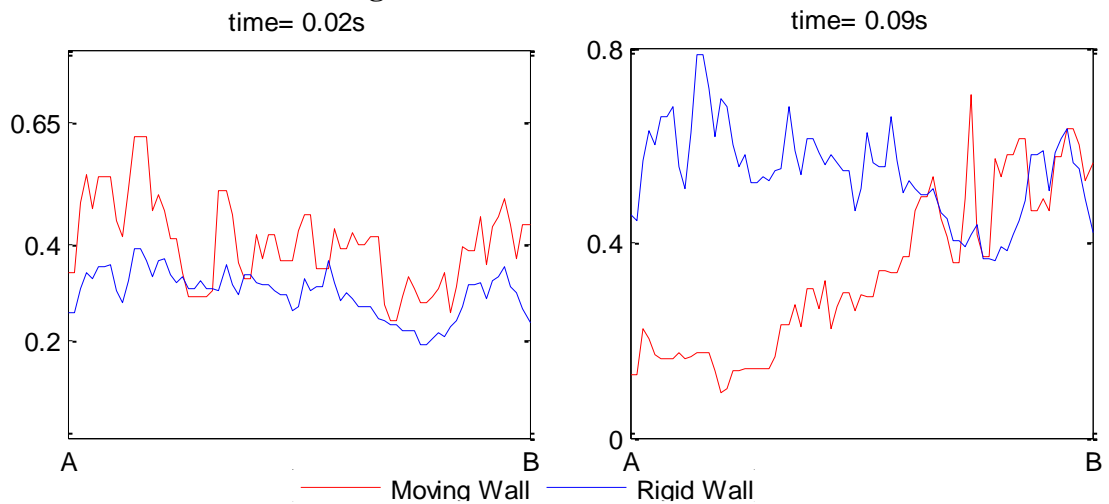**Figure 7.27.a :**Difference at time=0.02s    **Figure 7.27.b :**Difference at time=0.09s
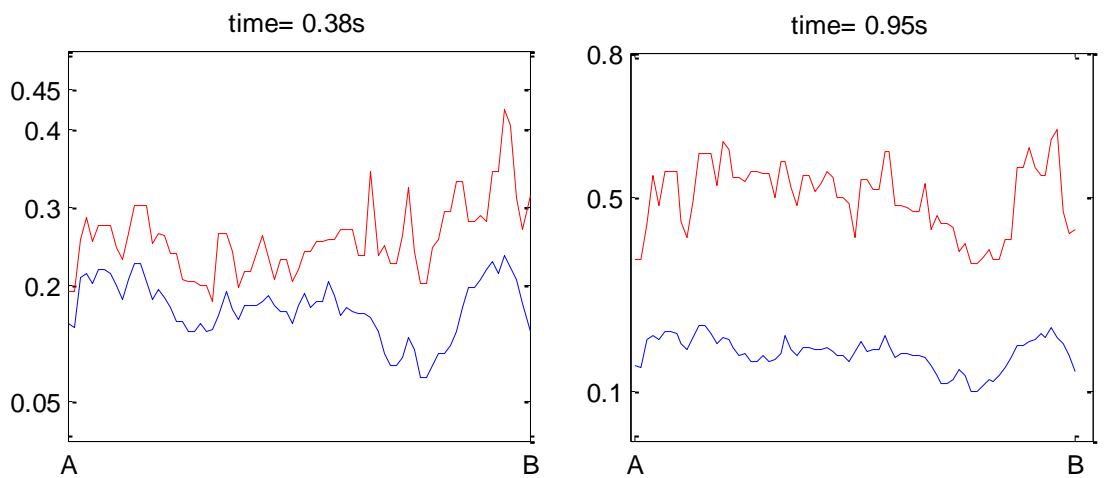


time= 0.38s



time= 0.95s

**Figure 7.27.c** :Difference at time=0.38s    **Figure 7.27.d** :Difference at time=0.95s

## 8. CONCLUSION

In blood flow simulations with low Reynolds number, the importance of non-Newtonian properties are effected by some factors. One of these factors is the geometrical properties of the artery. At the bifurcation and narrowing zones of arteries, the non-Newtonian effects are small due to the high shear rate at these regions. Another factor is the magnitude of an instantaneous velocity at the velocity inlet profile. For example, at t=0.09 sec. the velocity profile has maximum value so, the differences between non-Newtonian and Newtonian models are minimum.

On the other hand, no big differences on the velocity profiles of non-Newtonian and Newtonian are appeared and the maximum effect of non-Newtonian properties are observed on the center-line of the vessel according to the lower shear rate.

The Carreau and the Generalised Power Method generate higher viscosity at lower shear rates thus, these two models predict higher WSS distribution than that of the Newtonian model. But, at higher shear rates, the results of the Generalised Power Method converged to the results of Newtonian more quickly than the Carreau model. This feature is directly related to the mathematical formulation of the Generalised Power Method and the Carreau model.

The Casson model predicts lower WSS values than the other non-Newtonian models because at low and middle shear rates its viscosity smaller than those of the Carreau and the Generalised Power Method as it can be seen in the figure of apperant viscosity. At high shear rates the viscosity of Casson is a little above of the Newtonian viscosity and it does not converge to the Newtonian viscosity. As a result of this at the region with high shear rates the difference rate does not decrease while the difference of the others decreases.

# REFERENCES

[1] **Ballyk, P., D., Steinman, D., A., and Ethier, C., R.,** 1994: Simulation of Non-Newtonian Blood Flow in an End-to-Side Anastomosis. *Biorheology*, **31**, 565–586.

[2] **O'Callaghan, S., Walsh, M., and McGloughlin, T.,** 2006: Numerical Modeling of Newtonian and non-Newtonian Representation of Blood In A Distal End-To-Side Vascular Bypass Graft Anastomosis, *Medical Engineering & Physics*, **28**, 70-74.

[3] **Leuprecht, A., Perktold, K.,** 2000: Computer Simulation of Non-Newtonian Effects on Blood Flow in Large Arteries, *Computer Methods in Biomechanics and Biomedical Engineering,* **4**, 149-163.

[4] **Siauw, W., L., Ng, E., Y., K., and Mazumdar, J.,** 2000: Unsteady Stenosis Flow Prediction: A Comparative Study of Non-Newtonian Models With Operator Splitting Scheme, *Medical Engineering & Physics,* **22**, 265-277.

[5] **Cho, Y., I., and Kensey, K., R.,** 1991: Effects of the non-Newtonian Viscosity of Blood on Hemodynamics of Diseased Arterial Flows: Part 1, Steady Flows, *Biorheology,* **28**, 241-262.

[6] **Chan, W., Y., Ding, Y., Tu, Y., J.,** 2006: Modeling of Non-Newtonian Blood Flow Through a Stenosed Artery Incorporating Fluid-Structure Interaction, European Marketing Conference.

[7] **Valencia, A., Zarate, A., Galvez, M., and Badilla, L.,** 2006: Non-Newtonian Blood Flow Dynamics In A Right Internal Carotid Artery With A Saccular Aneurysm, *International Journal For Numerical Methods in Fluids,* **50**, 751-764.

[8] **Lukacova-Medvidova, M., Zauskova, A.,** 2007: Numerical Modelling of Shear-Thinning Non-Newtonian Flows In Compliant Vessels, *International Journal For Numerical Methods in Fluids,* **32**, 351-355.

[9] **Chen, J., Lu, X., Y., and Wang, W.,** 2005: Non-Newtonian Effects of Blood Flow On Hemodynamics In Distal Vascular Graft Anastomoses, *Journal of Biomechanics,* **39**, 1983-1995.

[10] **Chen, J., and Lu, X., Y.,** 2006: Numerical Investigation of the Non-Newtonian Pulsatile Blood Flow In A Bifurcation Model With a Non-Planar Branch, *Journal of Biomechanics,* **39**, 818-832.

[11] **Chen, J., and Lu, X., Y.,** 2004: Numerical Investigation of the Non-Newtonian Pulsatile Blood Flow In A Bifurcation Model With a Non-Planar Branch, *Journal of Biomechanics,* **37**, 1899-1911.

[12] **Goubergrits, L., Wellnhofer, E., and Kertzscher, U.,** 2008: Choice and Impact of a Non-Newtonian Blood Model for Wall Shear Stress Profiling of Coronoray Arteries, NBC 2008, **20**, 111-114.

**[13] Amornsamankul, S., Wiwatanapataphee, B., Wu, Y., H., Lenbury, Y.,** 2006, Effect of Non-Newtonian Behaviour of Blood on Pulsatile Flows in Stenotic Arteries, *International Journal of Biomedical Science,* **1**, 1306-1216.

**[14] Sultanov, R. A., Guster, D., Engelbrekt, B., and Blankenbecler, R.,** 2008: 3D Computer Simulations of Pulsatile Human Blood Flows in Vessels and in the Aortic Arch: Investigation of Non-Newtonian Characteristics of Human Blood. 11th IEEE International Conference on Computational Science and Engineering.

**[15] Boyd, J., Buick, J., M., and Green, S.,** 2007: Analysis of the Casson and Carreau-Yasuda non-Newtonian blood models in steady and oscillatory flows using the lattice Boltzmann method, *Physics of Fluids.,* **19**, 1070–6631.

**[16] Johnstona, B., M., Johnstona, P., R., Corneyb, S., and Kilpatrick, D.,** 2004: Non-Newtonian Blood Flow In Human Right Coronary Arteries: Steady State Simulations, *Journal of Biomechanics,* **37**, 709-720.

**[17] Johnstona, B., M., Johnstona, P., R., Corneyb, S., and Kilpatrick, D.,** 2006: Non-Newtonian Blood Flow In Human Right Coronary Arteries: Transient Simulation, *Journal of Biomechanics,* **39**, 1116-1128.

**[18] Gijsen, F., J., H., van de Vosse, F., N., and Janssen, J., D.,** 1999: The Influence of the Non-Newtonian Properties of Blood on the Flow In Large Arteries: Steady Flow In A Carotid Bifurcation Model, *Journal of Biomechanics,* **32**, 601-608.

**[19] Baaijens, J., P., W., Van Steenhoven, A., A., and Janssen, J., D.,** 1993: Numerical Analysis of Steady Generalised Newtonian Blood Flow In a 2D Model of the Carotid Artery Bifurcation, *Biorheology,* **30**, 63-74.

**[20] Fung, Y., C.,** 1993: Biomechanics: Mechanical Properties of Living Tissues, 2th Edition, Springer-Verlag, Newyork,USA.

**[21] Piskin, S., and Celebi, M., S.,** 2003: A Carotid Artery Bifurcation Model for Blood Flow, *7th Int. Symp. On Fluid Control, Mesurement and Visualization (FLUCOME '03),* Sorrento, Italy, August 25-28.

**[22] Piskin, S., Aribas, E., and Celebi, M., S.,** 2009: Coupled Simulation of a Carotid Artery Bifurcation Model, *10th Mesh Based Parallel Code Coupling Interface User Forum,* Sankt Augustin, Germany, Februry 17-18.

**[23] Aribas, E., Piskin, S., and Celebi, M., S.,** 2009: 3D Blood Flow Simulation In Human Arterial Tree Bifurcation, *14th National Biomedical Engineering Meeting,* (BIYOMUT 2009), May 20-22.

**CURRICULUM VITAE**

**Candidate's full name:**   Hasret TÜRKERİ

**Place and date of birth:**   05.06.1983

**Permanent Address:**   Karadeniz mh. 1129. Sk. No:8 Gaziosmanpaşa-Istanbul

**Universities and
Colleges attended:**

Istanbul Technical University, Mathematical Engineering, (2001-2007)

**Publications:**

▪ **Turkeri, H**., Piskin, S., and M. S. Celebi, 2010: Non-Newtonian Blood Flow Simulation in A Realistic Artery Domain, *5th Europen Conference on Computational Fluid Dynamics,* June 14-17, Lisbon, Portugal.